AD-A035 480 RAYTHEON CO SUDBURY MASS EQUIPMENT DIV F/G 20/5
SLANT RANGE VISIBILITY MEASURING LIDAR.(U)
SEP 76 R G MCMANUS, A A CHABOT, R M YOUNG F19628-75-C-0021
UNCLASSIFIED ER76-4355 AFGL-TR-76-0262 NL

1 OF 1
AD A035480

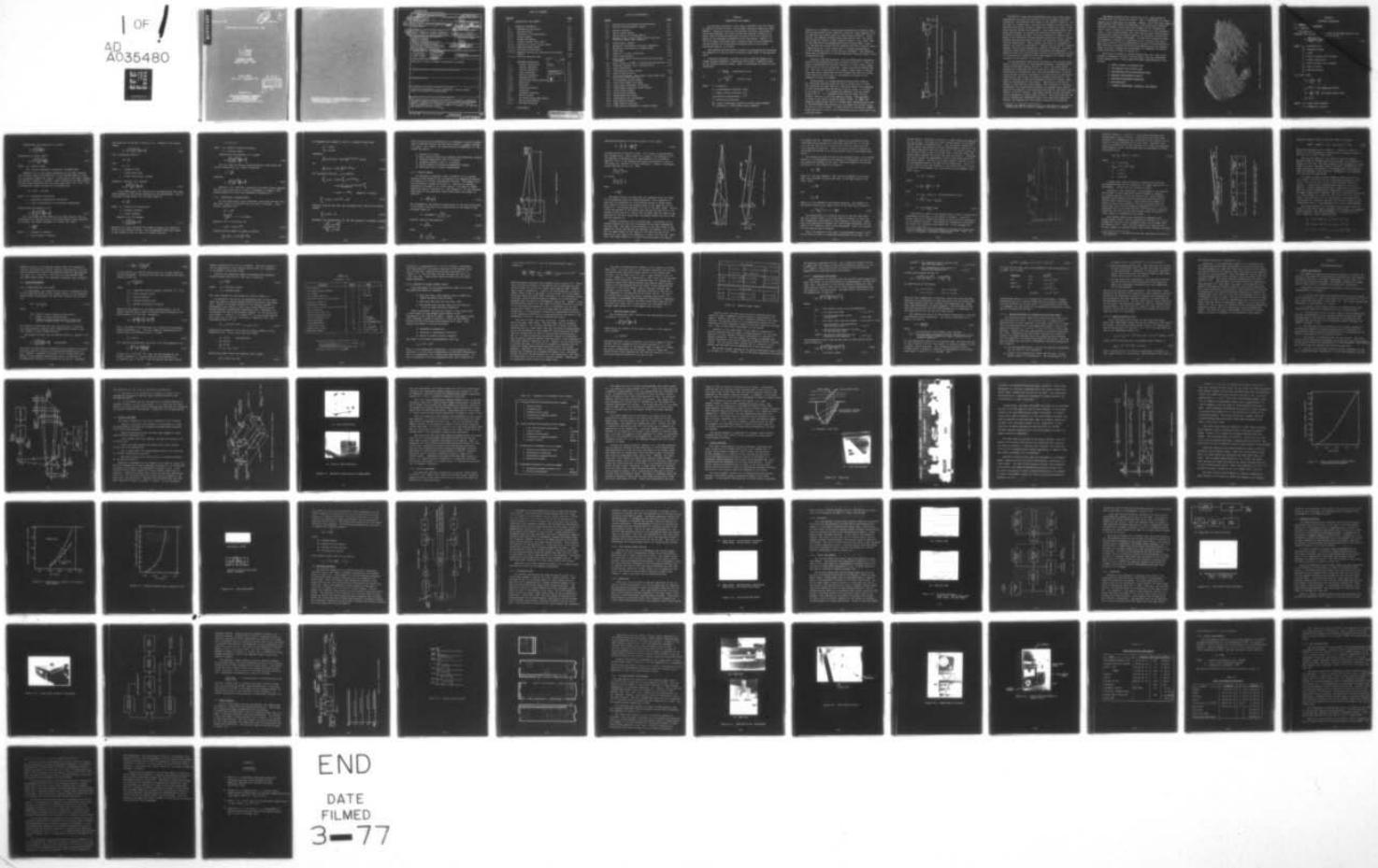

END

DATE FILMED
3-77

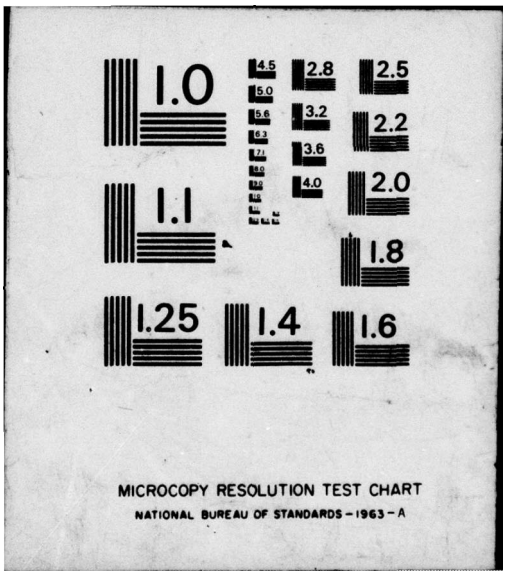
1.0
1.1
1.25
1.4
1.6
1.8
2.0
2.2
2.5
2.8
3.2
3.6
4.0
4.5
5.0
5.6
6.3
7.1
8.0
MICROCOPY RESOLUTION TEST CHART
NATIONAL BUREAU OF STANDARDS - 1963 - A

AFGL-TR-76-0262

ER76-4355

SLANT RANGE VISIBILITY MEASURING LIDAR

by

R. G. McManus
A. A. Chabot
R. M. Young
L. R. Novick

RAYTHEON COMPANY
EQUIPMENT DIVISION
Sudbury, Mass. 01776

FINAL REPORT
JULY 1974 - SEPTEMBER 1976

Prepared for

AIR FORCE GEOPHYSICS LABORATORY
AIR FORCE SYSTEMS COMMAND
UNITED STATES AIR FORCE
Hanscom A.F.B., Massachusetts 01731

UNCLASSIFIED

SECURITY CLASSIFICATION OF THIS PAGE (When Data Entered)

REPORT DOCUMENTATION PAGE	READ INSTRUCTIONS BEFORE COMPLETING FORM
1. REPORT NUMBER: AFGL-TR-76-0262	2. GOVT ACCESSION NO. / 3. RECIPIENT'S CATALOG NUMBER
4. TITLE (and Subtitle): SLANT RANGE VISIBILITY MEASURING LIDAR, FINAL REPORT	5. TYPE OF REPORT & PERIOD COVERED: FINAL REPORT, Jul 1974-Sept 1976; 6. PERFORMING ORG. REPORT NUMBER: ER76-4355
7. AUTHOR(s): Ralph G. McManus, Arthur A. Chabot, Robert M. Young Leonard R. Novick	8. CONTRACT OR GRANT NUMBER(s): F19628-75-C-0021
9. PERFORMING ORGANIZATION NAME AND ADDRESS: Raytheon Company, Boston Post Road, Sudbury, Massachusetts 01776	10. PROGRAM ELEMENT, PROJECT, TASK AREA & WORK UNIT NUMBERS: 62101F, 66700403
11. CONTROLLING OFFICE NAME AND ADDRESS: Air Force Geophysics Laboratory, Hanscom AFB, Massachusetts 01731, Monitor/Eugene Y. Moroz/LYP	12. REPORT DATE: Sept 1976; 13. NUMBER OF PAGES: 84
14. MONITORING AGENCY NAME & ADDRESS (if different from Controlling Office): 84 p. 6670 1204	15. SECURITY CLASS. (of this report): UNCLASSIFIED; 15a. DECLASSIFICATION/DOWNGRADING SCHEDULE

16. DISTRIBUTION STATEMENT (of this Report)

Approved for public release; distribution unlimited.

17. DISTRIBUTION STATEMENT (of the abstract entered in Block 20, if different from Report)

18. SUPPLEMENTARY NOTES

19. KEY WORDS (Continue on reverse side if necessary and identify by block number)

Visibility measurement in fog, eye-safety, optical design, ultra-violet laser, photomultiplier.

20. ABSTRACT (Continue on reverse side if necessary and identify by block number)

This design report presents the results of efforts to establish equipment parameters required for a single-ended transmissometer system to measure the visibility along a slant range such as that corresponding to the line of sight of a pilot in an aircraft approaching an airport runway.

DD FORM 1 JAN 73 1473 EDITION OF 1 NOV 65 IS OBSOLETE

UNCLASSIFIED

SECURITY CLASSIFICATION OF THIS PAGE (When Data Entered)

405 030

TABLE OF CONTENTS

LIST OF ILLUSTRATIONS

SECTION 1

INTRODUCTION AND SUMMARY

The material presented in this Report represents the Final Report on Contract F19628-75-C-0021, "Slant Range Visibility Measuring LIDAR System". During the course of the program, two design evaluation reports were published, and these contain the detailed information on which critical decisions were made, and which led to the nature and design of the equipment subsequently built and tested. However, so that this report may stand alone, important areas will be summarized. Further details can be obtained by referring back to the design evaluation reports, if desired.

The feasibility demonstration system to be discussed was developed in response to a need for slant visibility range (SVR) in the approach zone.

Visibility equipment currently in use at airports measure horizontal surface atmospheric transmission from which a parameter known as the "Runway Visibility Range" (RVR) is calculated, by either of two algorithms:

$$V = \frac{R \ln \varepsilon}{\ln T_R} \quad \text{(Koschmieder's Law)} \qquad (1\text{-}1)$$

or:

$$E_T = \frac{I(T_R)^{V/R}}{V^2} \quad \text{(Allard's Law)} \qquad (1\text{-}2)$$

where: V = visibility

R = transmissometer baseline length

ε = human contrast threshold (5%)

T_R = measured transmittance ($e^{-R\sigma}$)

σ = extinction coefficient

E_T = visual-illuminance threshold of pilot (mile-candles)

I = intensity of runway edge lights (candles)

Equation 1-1 is based on using contrast between an unlighted object and its background as the visibility criterion, while equation (1-2) is used when the runway lights are used as the criterion. During the day, the equation yielding the larger RVR is used. At night, when lights are used as visual targets, Allard's law is used. RVR is then defined as the maximum horizontal distance that a pilot will see down the runway from the approach end from a position above a specified point on its center line at a height corresponding to the average eye level of the pilot at touchdown. The parameter which must be measured to solve the empirical relations shown is the transmittance (T_R).

Typical of systems presently used are double-ended transmissometers of the Douglas-Young type, as shown in Figure 1-1, which require a transmitter and receiver mounted on 14-foot towers, separated by 250 or 500 foot distances. These are usually located some 500 - 600 feet to the side of the runway. Other types of sensors requiring taller towers must be even further away from the runway, since there are restrictions on the heights of towers in the immediate vicinity of runways.

Unfortunately, no system presently exists which measures the conditions existing along the pilot's actual line of sight. The visibility of real interest to the pilot during final approach is that encountered when the pilot's line of vision is inclined at an angle of 2° - 3° (standard ILS approach) with the runway surface and 9° - 15° (downward visual cut-off angle from the cockpit) with the line of the approach lights. This parameter is known as the "Slant Visibility Range" (SVR). An ideal SVR-measuring system would then be a single-ended transmissometer wherein the transmitter and receiver are co-located and transmit along the pilot's line of sight. A "Light Detection and Ranging (LIDAR)" system utilizing a laser as the transmitting source would seem to be a natural choice.

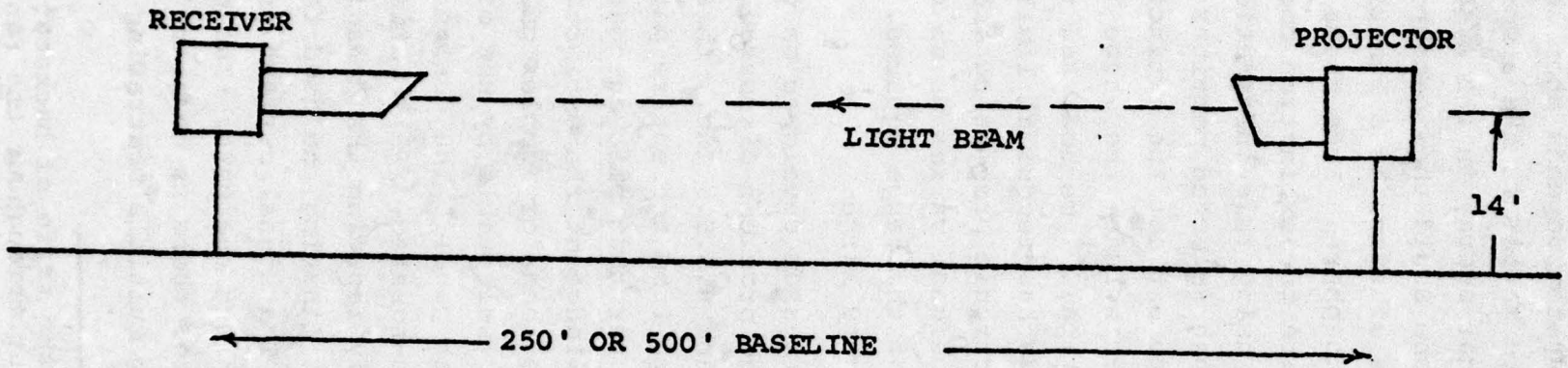

Figure 1-1. Douglas-Young Double-Ended Transmissometer

The use of a LIDAR SVR system depends upon laser energy being backscattered from particulate matter in the atmosphere (Mie backscattering), and detecting that energy in the system's receiver. In the case of a pulsed laser, one would then measure the energy backscattered from narrow volumes of space as a function of time, as the pulse travels through the atmosphere. From these measurements, one would then attempt to calculate the extinction coefficient (σ) as a function of range; and then, using this information, produce estimates of the visibility through selected portions of space. Several methods have been developed to extract the extinction coefficient from the LIDAR signal. These include: the shape (or signature)[1] method; the slope (or S-function)[2] method; and the ratio[3] method. However, each of these methods has technical limitations, and each requires a great deal of electronic processing and computation. In addition, since the received signal varies as an exponential function of σ and also as a function of the range squared, the dynamic range required of the receiver is very large.

The SVR-measuring LIDAR system developed on this program represents a unique solution to the problems discussed. Designed and developed by Raytheon Company and H.S.S., Inc., this LIDAR system measures the integrated return from the entire path of interest and determines the transmission over that path automatically, on every pulse, without any prior knowledge of the extinction and backscatter coefficients, and without the need for complex calculations. The range of interest is operator selectable by use of a digital thumbwheel on the processor's front panel. The design of the optical system is such that the range-squared, (R^2), variation is optically eliminated, thus significantly reducing the dynamic range requirements of the receiver, and eliminating the need for electronic accountability of the R^2 function. The signal current is then influenced only by atmospheric effects along the path. The system does not require a homogeneous atmosphere;* there is no near-field limitation problem; and degradation from multiple scattering is minimized.

* However, one assumes that the ratio of backscatter to attenuation coefficients (Φ) is constant throughout the range of interest.

The system transmits short ultraviolet (U.V.) laser pulses at a maximum rate of 10 pulses per minute. Thus, a measurement of transmission can be made every six seconds. However, since the actual measurement requires only several microseconds, a new range may be selected manually in-between every pulse, and thereby plot the transmission over a series of ranges to determine the homogeneity of the atmosphere (fog). In an ultimate system, one could vary the range automatically. An ultraviolet laser was chosen because it is eye-safe, and has good correlation with visible wavelengths. In this first feasiblity model, the equipment is housed in a custom-built van to protect the equipment and to allow it to be transported to any site for experimentation. The relatively low-provile van would then transmit up at an elevated angle to a point intersecting the Category I or Category II decision height altitudes, as shown in Figure 1-2.

The theory of operation, system descriptions, etc., will be developed in subsequent sections of this report. The main advantages of the Raytheon-H.S.S. single-ended SVR LIDAR transmissometer are as follows:

- SAFELY LOCATED IN APPROACH ZONE
- SVR MEASURED OVER A SLANT PATH
- SVR MEASURED OVER NON-HOMOGENEOUS PATH
- MEASURES TRANSMITTANCE DIRECTLY
- SIMPLIFIED ELECTRONIC PROCESSING
- HIGH DATA RATE
- AUTOMATIC MEASUREMENT, RECORDING, AND DISPLAY

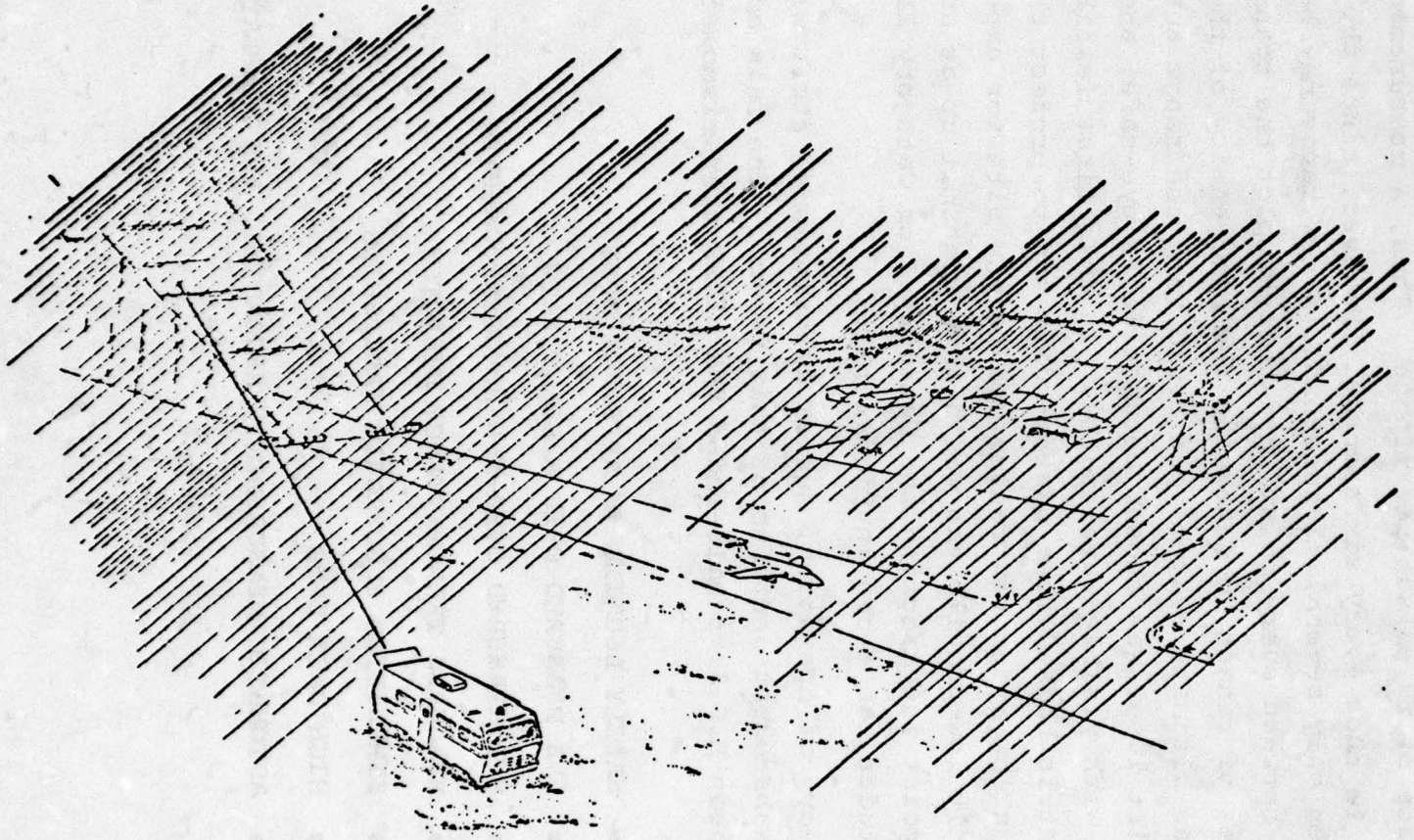

Figure 1-2. Portable Transmissometer Concept

SECTION 2

TECHNICAL DISCUSSION

2.1 MATHEMATICAL DERIVATION

2.1.1 RECEIVED [illegible]

The power returned from a target in any radar system is determined from the radar range equation to be:

$$P_r = \left(\frac{P_t G_t}{4\pi R^2}\right)\left(\frac{\rho G_i A_t}{4\pi R^2}\right) A_r \qquad (2\text{-}1)$$

where: P_r = received power

P_t = transmitted power

R = range

G_t = gain of antenna over isotropic

ρ = target reflectivity

G_i = gain of target over isotropic

A_t = area of target

A_r = area of receiver

In a laser radar:

$$G_t = \frac{4\pi}{\frac{\pi}{4}\theta_1^2} = \frac{16}{\theta_1^2}$$

$$G_i = \frac{4\pi}{\pi} = 4 \text{ (for Lambertian Target)}$$

$$A_t = \frac{\pi}{4}\left(\theta_1^2 R^2\right) \text{ (for target} \geq \text{laser beam)}$$

$$A_r = \frac{\pi}{4} D^2$$

where: θ_1 = laser beam divergence

D = diameter of receiver

Substituting into Equation (2-1) yields:

$$P_r = \left(\frac{\pi P_t D^2}{4R^2}\right)\left(\frac{\rho}{\pi}\right) \qquad (2\text{-}2)$$

Accounting for system losses:

$$P_r = \left(\frac{\pi P_t D^2 \eta_o T^2}{4R^2}\right)\left(\frac{\rho}{\pi}\right) \qquad (2\text{-}3)$$

where: η_o = optical losses

T^2 = two-way atmospheric attenuation (transmittance)

Equation (2-3) is the normal expression for the power received from a "hard" target of reflectivity ρ which scatters back in a cone of π steradians (Lambertian target). In the case of the LIDAR, however, the target is actually a "volume" of space defined by the beam diameter and that range associated with the laser pulse width ($\Delta R = c\tau/2$). For a "volumetric" target, the term ρ/π is replaced by:

$$\frac{\rho}{\pi} = \beta(\Delta R) = (\Phi\sigma)(\Delta R)$$

where: β = backscatter coefficient

σ = extinction (attenuation) coefficient

Φ = ratio of backscatter to attenuation coefficients

Substituting into Equation (2-3):

$$P_r = \left(\frac{\pi P_t D^2 \eta_o T^2}{4R^2}\right)\left(\Phi\sigma(\Delta R)\right) \qquad (2\text{-}4)$$

Now, the unique optical design of this LIDAR system is the incorporation of an aperture stop in the focal plane of such dimensions as to modify the normal throughput by a factor "K", where:

$$K = \left(\frac{dR}{fD}\right)^2 \qquad (2\text{-}4a)$$

where: d = diameter of aperture

f = focal length of receiver

This term will be derived in Section 2.1.3. Equation (2-4) now becomes:

$$P_r = \left(\frac{\pi P_t d^2 \eta_o T^2}{4f^2}\right)\left(\Phi\sigma(\Delta R)\right) \qquad (2\text{-}5)$$

But, as explained earlier:

$$\Delta R = \frac{c\tau}{2} ,$$

and:

$$P_t\tau = E$$

where: c = speed of light

τ = laser pulse width

E = laser pulse energy (joules)

Therefore: Equation (2-5) becomes:

$$P_r = \left(\frac{\pi E d^2 \eta_o T^2}{8f^2}\right)\left(c\Phi\sigma\right) \qquad (2\text{-}6)$$

In the LIDAR system, the detectors are photomultiplier (PM) tubes, which respond to light photons impinging on the photosurface. The relationship between photon flux and input power is:

$$N_s = \frac{P_r}{h\vartheta}$$

where: N_s = photon flux (photons/sec)

h = Planck's constant

ϑ = laser frequency

Equation (2-6) now becomes:

$$N_s = \left(\frac{\pi E d^2 \eta_o}{8f^2 h\vartheta}\right)\left(c\Phi\sigma T^2\right) \qquad (2\text{-}7)$$

Equation (2-7) then represents the number of photons per second arriving at the detector surface. The corresponding electrical output at the cathode of the P.M. tube is a current given by:

$$i_s = N_s \eta_d q$$

where: η_d = detector quantum efficiency

q = electron charge

Substituting into Equation (2-7) yields:

$$i_s = \left(\frac{\pi E \eta_o \eta_d d^2 q}{8 f^2 h \vartheta}\right)\left(c \Phi \sigma T^2\right) \tag{2-8}$$

But P.M. tubes are usually characterized by a term called the current responsivity (r_c), which is given by:

$$r_c = \frac{\eta_d q}{h \vartheta}$$

Therefore:

$$i_s = \left(\frac{\pi E r_c \eta_o d^2}{8 f^2}\right)\left(c \Phi \sigma T^2\right) \tag{2-9}$$

Equation (2-9), therefore, represents the signal current expected from any given pulse from a volume of atmosphere at range R, after having suffered the round trip atmospheric attenuation T^2.

2.1.2 DERIVATION OF TRANSMITTANCE

In this LIDAR system, major advantages accrue from the fact that the return signal is integrated over the path of interest. First, however, recognize that:

$$T^2 = e^{-2\sigma R}$$

$$\frac{\pi E r_c \eta_o d^2}{8 f^2} = C = \text{a constant}$$

Equation (2-9) is now written as:

$$i_s(R) = (Cc\Phi\sigma) e^{-2\sigma R} \tag{2-10}$$

Integrating with respect to range (R) yields:

$$\int i_s(R)\, dR = (Cc\Phi\sigma) \int e^{-2\sigma R} dR \tag{2-11}$$

To integrate with respect to time (t), recognize again that:

$$R = (c/2)t$$

$$dR = (c/2)dt$$

Therefore:

$$\int i_s(t)(c/2)dt = (Cc\Phi\sigma)\int e^{-2\sigma(c/2)t}\,(c/2)dt \qquad (2\text{-}12)$$

or:

$$\int i_s(t)dt = (Cc\Phi\sigma)\int e^{-2\sigma(c/2)t}dt \qquad (2\text{-}13)$$

For the period from time t_1 to infinity:

$$\int_{t_1}^{\infty} i_s(t) = (Cc\Phi\sigma)\int_{t_1}^{\infty} e^{-2\sigma(c/2)t}dt$$

$$= (Cc\Phi\sigma)\left(\frac{1}{-2\sigma(c/2)}\right)e^{-2\sigma(c/2)t}\Big|_{t_1}^{\infty}$$

$$= (-C\Phi)(o - e^{-2\sigma R_1}) \qquad (\text{where } R_1 = (c/2)t_1)$$

$$\int_{t_1}^{\infty} i_s(t)dt = C\Phi e^{-2\sigma R_1} = C\Phi T^2 \qquad (2\text{-}14)$$

Similarly, one can show that the integration from time t=o to infinity yields:

$$\int_o^{\infty} i_s(t)dt = C\Phi \qquad (2\text{-}15)$$

Therefore, the transmittance (T) over the interval of interest is simply:

$$T = \left(\frac{\int_{t_1}^{\infty} i_s(t)dt}{\int_o^{\infty} i_s(t)dt}\right)^{1/2} \qquad (2\text{-}16)$$

This is the gist of the Raytheon-H.S.S. technique, in which transmittance is derived directly on every pulse without a priori knowledge of σ and β. As a result, the steps required to determine T in this system are merely:

- Transmit U.V. pulse
- Split received signal into numerator and denominator channels
- Integrate denominator from 0 to infinity
- Integrate numerator from t_1 to infinity
- Divide numerator integral by denominator integral
- Take square root to yield transmittance

2.1.3 OPTICAL ANALOG

As indicated in Equation (2-4a) of Section 2.1.1, a unique feature of this system is the utilization of an appropriate aperture to eliminate the inverse range-squared function. The geometry for this derivation is shown in Figure 2-1. Here let us consider a scatterer in the beam to be a point source. Its image is formed behind the lens at a distance f_2. The diameter d', at the principal focal plane of the convergent bundle which forms that image, is given by:

$$d' = D\left(\frac{f_2 - f}{f_2}\right) \tag{2-17}$$

The throughput of the system is proportional to the area of the hole in the stop to the area of the cross-section of the bundle at the principal focus, or:

$$K = \text{throughput} = \frac{d^2 f_2^2}{D^2 (f_2 - f)^2} \tag{2-18}$$

However, from the lens equation:

$$R = \frac{f_2 f}{f_2 - f} \tag{2-19}$$

Thus:

$$\frac{R^2}{f^2} = \frac{f_2^2}{(f_2 - f)^2} \tag{2-20}$$

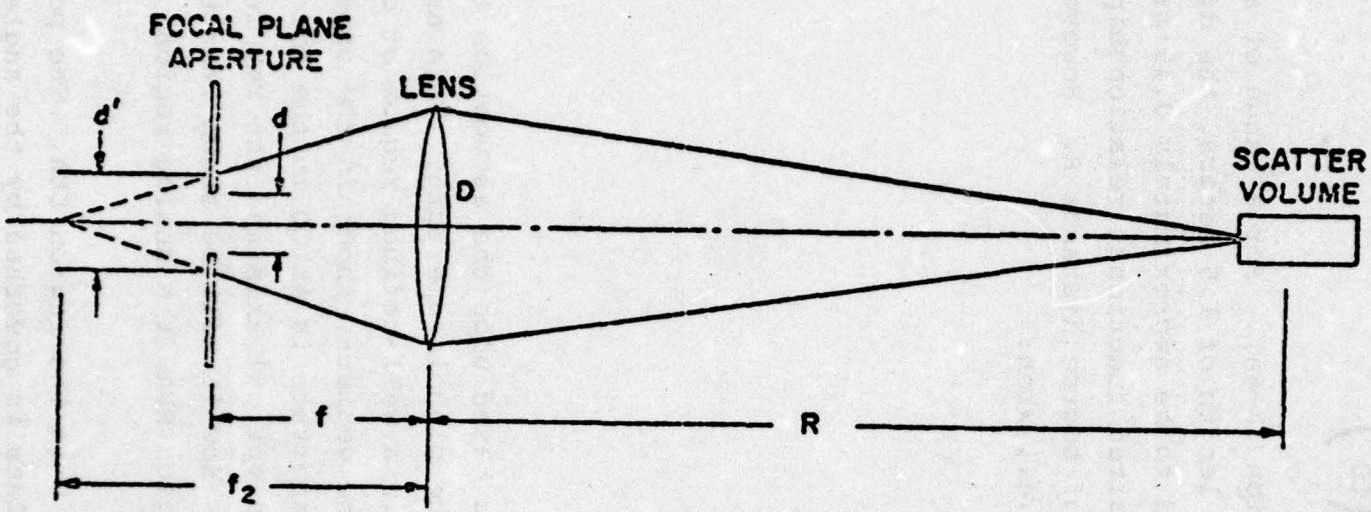

Figure 2-1. Receiver Geometry

Substituting Equation (2-20) into Equation (2-18) yields:

$$K = \frac{d^2}{D^2} \frac{R^2}{f^2} = \left(\frac{dR}{fD}\right)^2 \qquad (2\text{-}21)$$

as given earlier in Equation (2-4a). For a range of approximately one kilometer and a focal length of 1.5 meters, the diameter (d) of the aperture is calculated to be approximately 0.45 millimeter. Equation (2-21) is the desired functional relationship for gain in the analog as a function of source distance R. However, the method breaks down when $d' \leq d$; i.e., when:

$$\left(\frac{f_2 - f}{f_2}\right) D \leq d;$$

or, since:

$$\left(\frac{f_2 - f}{f_2}\right) = \frac{f}{R}$$

when:

$$R \geq \left(\frac{D}{d}\right) f$$

The above solution is based upon the assumption that the image of the scatterer covers the pinhole aperture. This assumption is true only for scatterers in a well-defined region of object space. This region is given by the geometry shown in the upper portion of Figure 2-2. The pinhole aperture is at CD in the focal plane. Point A is the intersection of the optical axis and the ray from point C refracted by the lens at B. Now it will be shown that the image of any scatterer in the conic region BEA, the analog region, will fully subtend the aperture CD.

Consider a scatterer S in the region BEA. The portion of its scatter collected by the lens is governed by the angle subtended by the lens, BSE. The image of the scatterer at the focal plane is the segment FG, since the rays SBF and SEG mark its borders. It is clear that the upper border of the image at F is above the top of the aperture at C as long as the scatterer S is below the line BA. Similarly, the lower border at G is below the bottom edge D as long as

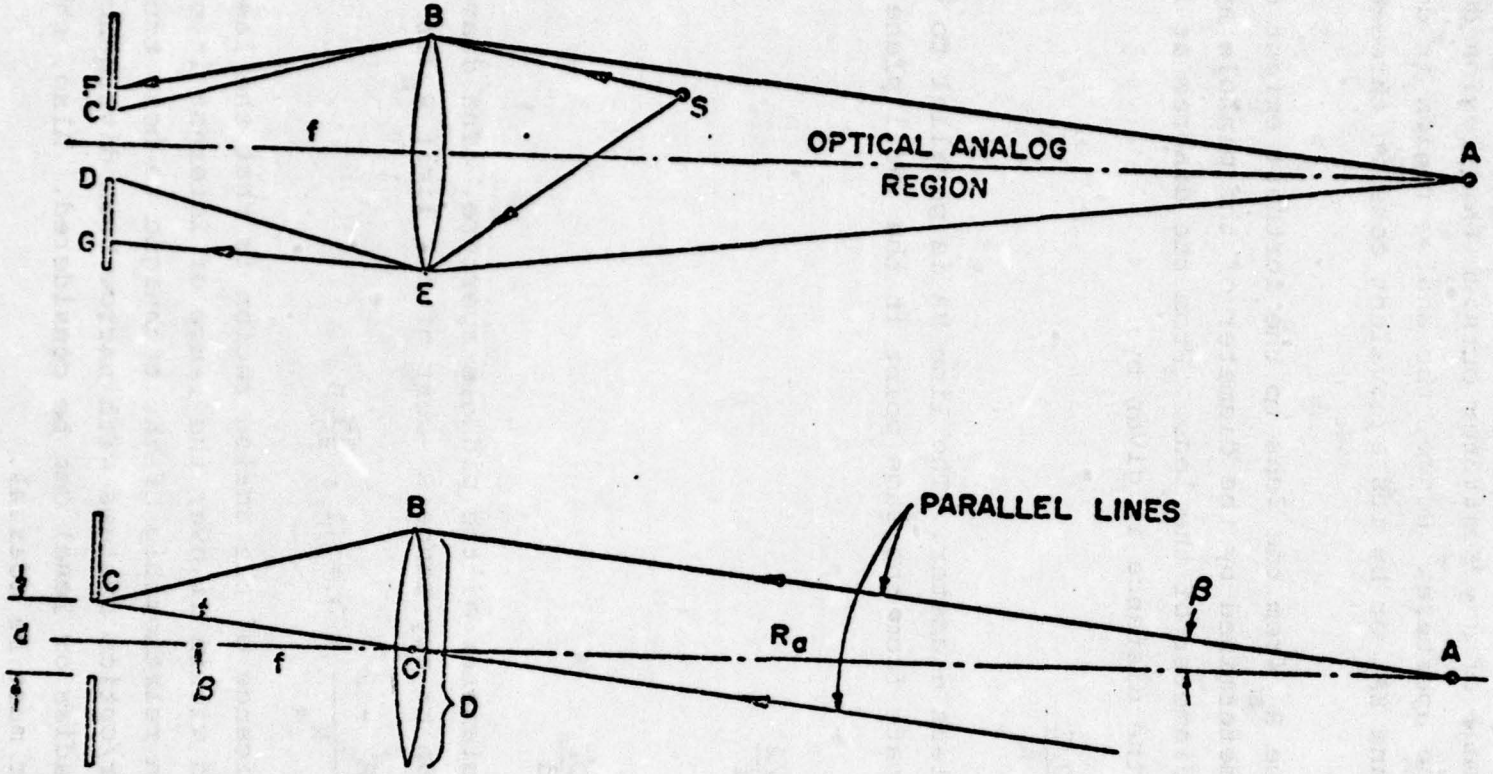

Figure 2-2. Optical Analog Region

S is above line EA. Therefore, the image of any scatterer in the region BEA fully subtends the focal-plane aperture CD. It is also true that the image of any scatterer outside this region does not fully subtend the aperture. Hence, the analog region is defined by the borders BA and EA, or by its equivalent cone in three-dimensional space.

The distance R_a from the lens to the furthest extent of the analog region at A is determined by the diameter of the pinhole and the focal length and diameter of the lens. From the diagram at the bottom of Figure 2-2, the distance is given by:

$$R_a = \frac{D/2}{\beta}$$

where D is the lens diameter. The line BA is parallel to CO since both rays originate from the same point in the focal plane of the lens. Thus:

$$\beta = \frac{d/2}{f}$$

and;

$$R_a = \frac{Df}{d} \qquad (2\text{-}22)$$

where d is the diameter of the pinhole aperture. The diameter of the analog region at any range R short of the limit R_a is given by:

$$D_a = \frac{R_a - R}{R_a} \times D = (1 - \frac{dR}{fD})D \qquad (2\text{-}23)$$

The significance of the analog region is that the laser beam must be confined within it over the range of interest in order for the transmission relationship of the technique to hold true. Therefore, only laser/optics systems with narrow beam divergences (of the order of 10^{-4} radian or less) can be considered. Also, the transmitter and receiver must be coaxial.

Thus, the geometry of the analog transmissometer places a limit on the range at which a transmission measurement can be made. The

analog region is re-drawn in Figure 2-3. Three ranges are depicted--R_a, R_b, and R_m. The range R_a is the furthest extent of the analog zone as derived in Equation (2-22). Only scatterers within this region fulfill the condition for the transmissometer equation, that the image completely cover the analog hole. The second range R_b is the furthest range at which the laser beam is confined within the analog region; beyond this region the beam overflows it. Therefore, the limit R_b marks the approximate limit to the useful portion of the analog region. Actually, R_b is made slightly shorter to allow for misalignment between the beam and the analog zone. Hence, it is the range at which the diameter of the analog zone (D_a) is equal to the laser beam diameter (D_1) plus twice the misalignment tolerance* (θ_{mis}):

$$D_a = D_1 + 2\theta_{mis}R_b \ .$$

Since:

$$D_a = \left(1 - \frac{R}{R_a}\right)D = D - \frac{dR}{f}$$

and;

$D_1 = \theta_1 R$, where θ_1 = laser divergence, then:

$$D - \frac{dR_b}{f} = \theta_1 R_b + 2\theta_{mis}R_b,$$

or;

$$R_b = \frac{D}{\theta_1 + 2\theta_{mis} + d/f} \qquad (2\text{-}24)$$

The range R_m, which is the maximum range at which a transmission measurement can be made, is the range of interest. It must be shorter than R_b by a sufficient margin to allow accurate integration of the numerator current. The smaller the attenuation coefficient, the longer the integration time should be. In the lightest fog

*It can be shown that the misalignment can be much worse before the error in measuring transmission becomes significant. Thus; this value of tolerance is extremely conservative.

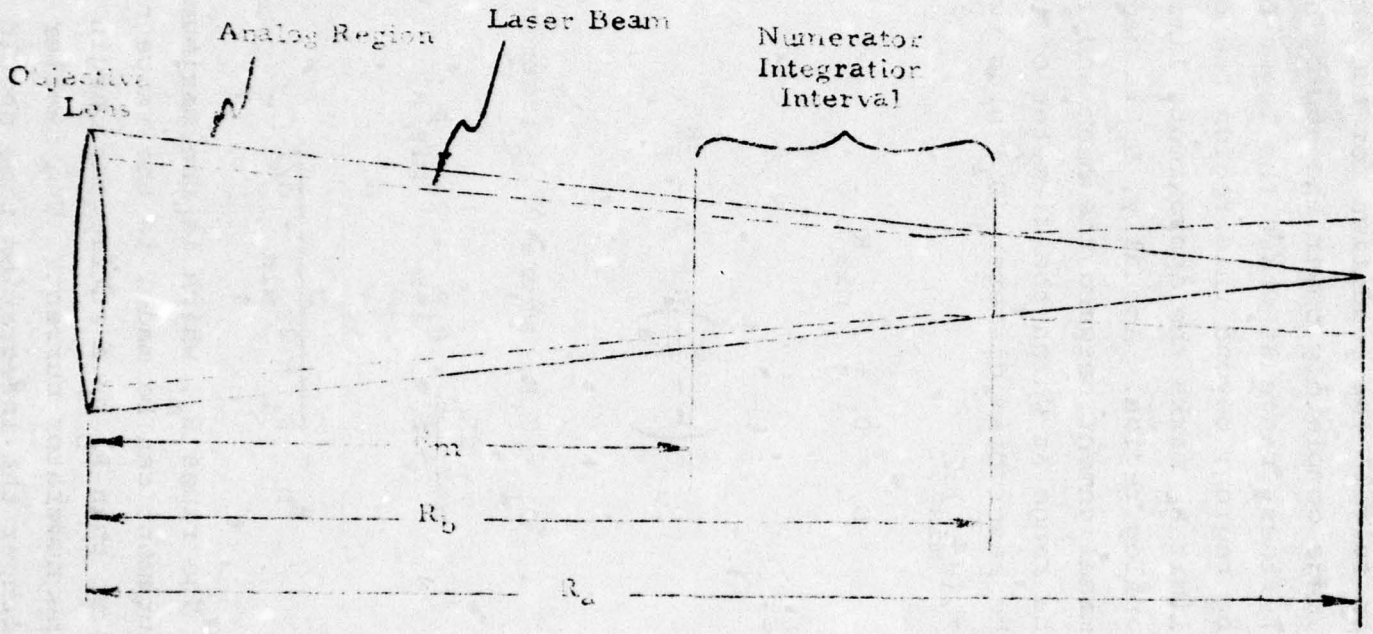

Figure 2-3. Analog Region of Transmissometer

condition,* where $\sigma = 0.002$ ft.$^{-1}$, the current decreases by 90 percent over a range of 600 ft. Since the current drops exponentially in a homogeneous fog, 90 percent of the integral out to infinity is also contained within this range. Therefore, the error is 10 percent in T^2 and 5 percent in T, which is acceptable. Using Equation (2-24), the maximum range of measurement is then calculated to be:

$$R_m = R_b - 600 \text{ ft.} = 1700 \text{ ft.} \qquad (2\text{-}25)$$

where:

$\theta_l = 10^{-4}$ rad

$\theta_{mis} = 1.3 \times 10^{-5}$ rad

D = 0.3 m

f = 1.5 m

d = 0.45 mm

In heavy fogs, where the range of operation is much less, the system provides for the insertion of a larger aperture of 4.5 millimeters. In this case, R_m becomes 230 feet.

According to FAA regulations, a pilot making an ILS approach must be able to see enough from decision height to complete his landing visually, or else he must pull up. High intensity approach lights aligned with the runway have been installed as landing aids at many airports. These lights are arranged in a series of rows or bars spaced at 100-foot intervals along the flight path, with the bars oriented perpendicular to it. It is considered that if the pilot can see a 500-foot span of approach-light bars (six bars) he will have enough visual information to orient himself to touchdown on the runway.

This concept leads to the definition of Approach Light Contact Height (ALCH), which is illustrated in Figure 2-4. It is assumed that the pilot has a downward visual cut-off angle from his cockpit of 15°. Thus, from the geometry, in order to see a 500-foot segment of approach lights from a given altitude, the pilot

---

* The range of σ of interest here has been specified as 0.002 ft^{-1} to 0.035 ft^{-1}.

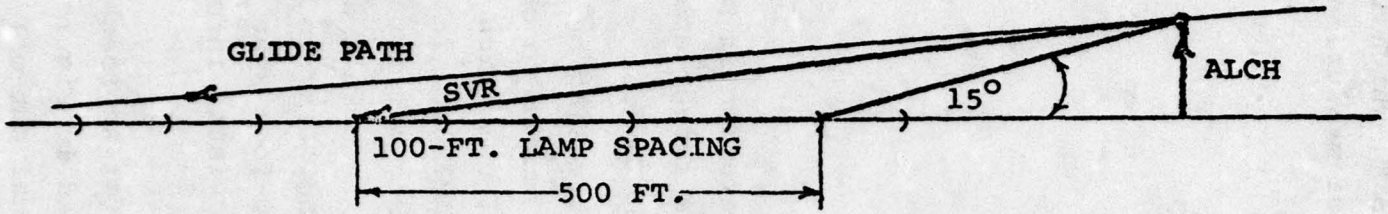

DECISION HEIGHT (FEET)	CATEGORY	MINIMUM SVR (FEET)
200	I	1,262
100	II	878

Figure 2-4. Approach Light Contact Height (ALCH) and Slant Visibility Range (SVR) Geometry

requires visibility over a slant path (SVR) of at least:

$$(SVR)^2 = (ALCH)^2 + (500 + ALCH \cot 15^\circ)^2 \text{ feet} \qquad (2\text{-}26)$$

The minimum required SVR to proceed to a landing is shown in Figure 2-4 for the Category I and Category II decision heights of 200 feet and 100 feet, respectively.

Allard's Law (Equation (1-2) would be used to translate measured values of transmittance over the slant path indicated in Figure 2-4 into SVR. The same principle could be applied to a SVR without the use of approach lights by locating suitable high contrast markings on the surface of the ground under the glide path where the approach lights would be. Koschmieder's Law (Equation 1-1) would then be appropriate.

It should be noted that the concept of ALCH and SVR take into account a vertical as well as horizontal component of visibility, and that the description did not include a method of sensing. A double-ended transmissometer might be practically adapted to measure transmittance over a slant path or a vertical path for strictly meteorological observations or experiments. The upper element would, however, constitute a hazardous obstruction if it were located on a tower near the glide path of an active runway. The desirability of a single-ended transmissometer for this function is indicated, and this has been the reason for the single-ended design of the Raytheon-H.S.S. LIDAR transmissometer.

The ranges required for the LIDAR transmissometer shown in Figure 2-4 are within those calculated for the analog zone geometry defined earlier. The ranges pertinent to the analog zone and their respective transit times are thus:

$$R_a = 1 \text{ km} = 3281 \text{ ft.}; \; \tau_a = 6.67 \times 10^{-6} \text{ sec}$$

$$R_b = 700 \text{ m} = 2300 \text{ ft}; \; \tau_b = 4.68 \times 10^{-6} \text{ sec}$$

$$R_m = 518 \text{ m} = 1700 \text{ ft.}; \; \tau_m = 3.46 \times 10^{-6} \text{ sec}$$

However, since R_b is the maximum useable range, the integration time for the denominator channel should be approximately 4.68 μsec; and the integration time for the numerator should be approximately 1.22 μsec (i.e., 4.68 μsec - 3.46 μsec) for that maximum range. For lower visual ranges, the numerator integration time increases.

2.2 SYSTEM PERFORMANCE

2.2.1 SIGNAL-TO-NOISE (S/N) RATIO

In this system, the signal-to-noise ratio of interest is that of the integrated signal current (signal charge) to the integrated noise current (noise charge) for which the (current) S/N is given as:

$$S/N = \frac{s}{(\bar{n} + s)^{1/2}} \qquad (2\text{-}27)$$

where:

S/N = ratio of signal charge to noise charge
s = number of signal photoelectrons
$\bar{n}$ = number of photoelectrons from the background and dark current within the integration time

This formula is based upon the fact that the noise is Gaussian (or, more precisely, Poisson) and is approximately equal to the total number of events (photoelectrons).

The photon flux rate (N_s) was derived earlier in Equation (2-7) to be:

$$N_s = \left(\frac{\pi E d^2 \eta_o}{8 f^2 h\vartheta}\right)\left(c\Phi\sigma T^2\right) \quad \text{(photons/sec)} \qquad 2\text{-}28)$$

The number of photoelectrons generated at the cathode of the photomultiplier tube is a function of its quantum efficiency(η_d); or $N_s\eta_d$. However, inspection of Equation (2-14) reveals that integration of the numerator channel from time t_1 to infinity is mathematically equivalent to dividing by the term $c\sigma$. Therefore:

$$s = \frac{N_s \eta_d}{c\sigma} = \frac{\pi E_d^2 \eta_o \eta_d \Phi T^2}{8 f^2 h\vartheta} \tag{2-29}$$

In this system, the dominant noise source will be that caused by the sky background. The photon flux rate (N_b) caused by the background is given as:

$$N_b = \frac{N_\lambda \Delta\lambda A_r \Omega_r \eta_r}{h\vartheta} \tag{2-30}$$

where:

N_λ = background spectral radiance (watts/m^2 - $\mathring{A}$ - ster)

$\Delta\lambda$ = filter spectral width

A_r = area of receiver

Ω_r = receiver field-of-view

η_r = optical efficiency of receiver

Because of the geometry of the analog transmissometer, the receiver field-of-view is equal to the solid angle subtended by the pinhole aperture at the lens. Therefore:

$$A_r \Omega_r = \left(\frac{\pi}{4} D^2\right)\left(\frac{\pi}{4} \frac{d^2}{f^2}\right) = \left(\frac{\pi}{4} \frac{dD}{f}\right)^2 \tag{2-31}$$

Again, the number of photoelectrons is a function of the detector quantum efficiency (η_d). The total number of photoelectrons collected during an integration time τ_i is then:

$$\bar{n}_b = N_b \eta_d \tau_i, \tag{2-32}$$

and, substituting Equations (2-30) and (2-31) into Equation (2-32):

$$\bar{n}_b = \left(\frac{N_\lambda \Delta\lambda \eta_r \eta_d \tau_i}{h\vartheta}\right)\left(\frac{\pi dD}{4f}\right)^2 \tag{2-33}$$

A value of 3×10^{-3} (w/m^2 - $\mathring{A}$ - ster) has been assumed for the spectral radiance N_λ. This is based on the measurements of G. Knestrick and J. Curcio[4] for the horizon sky under various

weather conditions from 0.38 to 1.0 micron. The value assumed is for an exceptionally clear overcast day at 1:00 P.M. Therefore, it is probably a worst case value.

Finally, the equivalent number of photoelectrons generated by dark current from the P.M. tube ($\bar{n}_d$) is given by:

$$\bar{n}_d = \frac{I_d \tau_i}{q} \tag{2-34}$$

where: I_d = tube dark current

q = electron charge

The values assumed for this system are listed in Table 2-1.

By definition, the S/N in the denominator will be very large, since the energy is being received starting effectively from range zero. However, the energy received in the numerator channel is considerably less, since it starts from a range downfield after having suffered a considerable transmission loss. Therefore, let us calculate the S/N of the numerator channel. In the minimum fog case, where $\sigma = 0.002$ ft.$^{-1}$ (0.006562 m^{-1}), at the maximum measurement range (R_m) of 1700 feet calculated in Equation (2-25), the transmission loss (T^2) is:

$$T^2 = e^{-2(0.002)(1700)} = 1.11378 \times 10^{-3} \tag{2-35}$$

Substitution of Equation (2-35) and the values of Table 2-1 into Equations (2-29), (2-33), and (2-34) will yield:

$s = 310.77$ photoelectrons

$\bar{n}_b = 82.7857$ "

$\bar{n}_d = 0.0019$ "

$\bar{n} = \bar{n}_b + \bar{n}_d = 82.79$ "

Substituting these values into Equation (2-27) yields:

$$S/N = 15.66 \ (23.9 \text{ dB}) \tag{2-36}$$

Table 2-1

Parametric Values

Parameter	Symbol	Value
Laser energy	E	5 mJ
Focal plane aperture diameter	d	0.45 mm
Focal length	f	1.5 m
Lens aperture diameter	D	30.48 cm
Atmospheric transmission to range R	T	
Attenuation coefficient	σ	
Backscatter coefficient	β	
Ratio of backscatter to attenuation coefficients	Φ	0.04 sr^{-1}
Optical efficiency	η_o	0.1125
Receiver optical efficiency	η_r	0.25
Detector quantum efficiency	η_d	0.2
Receiver integration time	τ_i	1.22 μsec
Energy per photon	$h\nu$	5.7×10^{-19} J
Background radiance	$N\lambda$	3×10^{-3} W/m^2-Å-sr
Spectral filter width	$\Delta\lambda$	50 Å
Detector dark current	i_d	2.5×10^{-16} A
Electronic charge		1.6×10^{-19} coul

The optical efficiency is determined as follows:

Two-way transmission of 50/50 beam splitter	0.25
Background filter transmission	0.5
Transmission of lens and mirror (two-way)	0.9

Thus, $\eta_o = 0.25 \times .5 \times .9 = 0.1125$

Similarly, a transmission of T = 2% (T^2 = 0.0004), the minimum value specified for this system, occurring at the maximum range (R_m) of 1700 feet, requires an extinction coefficient (σ) of 0.0023 $ft.^{-1}$. For this case, one can calculate the S/N to be 8.006 (18.1 dB). These values should be sufficient for proper system operation.

2.2.2 ANALYSIS OF SIGNAL CURRENT LEVELS

The requirements for the photomultiplier tubes in the LIDAR SVR System are basically threefold:

- They must have a wide dynamic range to handle the signal variation along the path.
- They must have fast rise and decay times.
- The maximum tube currents should not be exceeded, such as to cause prolonged saturation.

These requirements are much less severe in this system than in other types of single-ended lidars because of the elimination of the inverse R^2 effect. However, the signal current still undergoes a range of variation in spite of the pinhole aperture in the focal plane which cancels the R^2 term. Three factors contribute to the wide variation:

- Atmospheric transmission
- Variation of backscatter coefficient
- Choice of pinhole aperture diameter

The signal in the analog transmissometer varies as:

$$i_s \alpha \beta T^2 = \Phi \sigma T^2 \qquad (2\text{-}37)$$

where β is the backscatter coefficient, σ is the extinction coefficient, Φ is the ratio of backscatter to extinction coefficients, and T is transmission, all of which have been defined earlier. If one is interested in the 2% transmission point and a variation in

σ of 0.002 to 0.035 ft.$^{-1}$, then the required dynamic range in current is:

$$\frac{i_{max}}{i_{min}} = \frac{\Phi\sigma_{max}}{\Phi\sigma_{min}} \times \frac{1}{T^2_{min}} = \frac{0.035}{0.002} \times \frac{1}{(.02)^2} = 4.375 \times 10^4 \qquad (2\text{-}38)$$

Photomultipliers typically have a dynamic range of about 10^4. Therefore, for this and reasons of saturation (to be discussed shortly) we have chosen to use two P.M. tubes, splitting the signal between them, using a beamsplitter. Since it is the denominator (close-in) channel which is apt to saturate, it will receive 1% of the signal; while the remaining energy (99%) is passed on to the numerator which, of course, cannot afford attenuation, because it is the quantity measured after the effects of atmospheric extinction. However, since the denominator signal will have been artifically reduced by a factor of 99, the signal processor will have to compensate for the loss by electronic means. This can be accomplished by supplying appropriate gain in the denominator electronics; appropriate attenuation in the numerator electronics; or by accounting for the factor in the mathematical solution. The last approach was chosen.

The need for fast rise time is obvious. It must be able to follow the short laser pulse. The fast decay time is necessary for two reasons: (1) to follow the fall-off in signal with time (although this is a less severe task for the analog transmissometer due to the elimination of the inverse R^2 relationship and the fact that the current does not have to be monitored instantaneously); and (2), to avoid integrating any spurious signal on transmission such as may be caused by scatter from the optics, stray flashlamp or ruby laser (6943 Å) radiation, or rfi. However, as the calculations to follow will show, it will also be possible to saturate the P.M. tubes with energy backscattered internally within the optical assembly. Therefore, the start of integration for the denominator channel can be delayed by an appropriate amount (e.g., one pulse length) by having the denominator P.M. tube effectively "off" while the laser pulse is still witin the optical assembly. Measurement of transmission starts after this slight delay.

The type of photomultiplier chosen for this system is the RCA Model 4516. In a P.M. tube, it is extremely important that one does not exceed either the peak cathode current or the average anode current. For the Model 4516 P.M. tube, a peak cathode current of 1×10^{-8} ampere at a tube temperature of $22^{o}C$ should not be exceeded. Because of the sensitivity of the photocathode, the voltage drop caused by higher peak cathode currents may produce radial electric fields on the photocathode which can result in poor photoelectron collection in the first dynode. This is the most critical tube parameter in this system. The operating stability of the 4516 is also dependent on the magnitude of the anode current. The use of an average anode current well below a maximum rated value of 0.5 milliampere is recommended when stability of operation is important. In this application, however, the short laser pulse width and the relatively low pulse rate (10 per minute) will guarantee that an average anode current of 0.5 milliampere does not occur.

2.2.2.1 Expected Signal Levels

The instantaneous signal current at the photocathode was derived in Equation (2-9) to be:

$$i_s = \left(\frac{\pi E r_c \eta_o d^2}{8 f^2}\right)\left(c \Phi \sigma T^2\right) \qquad (2\text{-}39)$$

Substituting the constant values given in Table 2-1 into Equation (2-39) yields:

$$i_s = 66 d^2 \sigma T^2 \qquad (2\text{-}40)$$

The maximum signal occurs, naturally, at the very instant of transmission, when no attenuation has yet been suffered ($T^2 = 1$); and the minimum value occurs at the maximum range, or when $T^2 = 0.0004$, the limit of measurement for the system. Table 2-2 shows the signal current levels expected for the range of values of σ, and for two analog aperture diameters (0.45 and 4.5 mm).

d = 0.45 mm			
σ	$T^2 = 0$ (R = O)	$T^2 = 1.11378 \times 10^{-3}$ (R = 1700 ft.)	$T^2 = 4 \times 10^{-4}$
0.002	8.8×10^{-8}A	9.7×10^{-11}A	3.5×10^{-11}A
0.035	1.5×10^{-6}A	1.7×10^{-9}A	6.1×10^{-10}A
d = 4.5 mm			
0.002	8.8×10^{-6}A	9.7×10^{-9}A	3.5×10^{-9}A
0.035	1.5×10^{-4}A	1.7×10^{-7}A	6.1×10^{-8}A

Table 2-2. Expected Signal Levels

From the table, one sees that the signal currents would all exceed the peak recommended cathode current of approximately 10^{-8} ampere. However, with the 100 to 1 reduction affected by the beam-splitter, the current levels into the denominator channel are all effectively within acceptable limits for the small aperture (0.45 mm) case. This is the primary requirement for the system.

However, in very heavy fogs, if one wishes to penetrate to greater distances, one can insert a larger aperture. For the large aperture (4.5 mm), however, even more attenuation is required to prevent saturation. For this reason, the system is equipped with several attenuators which can be inserted in addition to the original (100/1). For the values shown, another 100 to 1 reduction is required, and this must also be accounted for in the electronics.

The minimum current expected at the maximum measurement range (1700 ft) is then 3.5×10^{-11} ampere. This is the value expected at the start o

the numerator integration period. This integration should continue at least until the current is an order of magnitude smaller, or 3.5 x 10^{-12} ampere. This value is well in excess of the noise current generated by the photomultiplier dark current.

2.2.2.2 Backscatter from Optics

Laser radiation is scattered from the system's 50/50 beamsplitter, lens, and mirror as the pulse leaves the transmissometer and from the light trap. The portion of this scatter passing through the focal plane aperture causes a high initial pulse lasting approximately for the duration of the laser pulse. The peak current from scatter off the beamsplitter is given by:

$$i_{scl} = \left(\frac{\pi r_c P d^2}{4}\right)\left(\frac{\eta_{01} g_1(90^\circ)}{x^2}\right) \qquad (2\text{-}41)$$

where:

i_{scl}	= the scatter current from the beamsplitter	
P	= the laser peak power	= 2.5 x 10^5 W
r_c	= the PM photocathode current responsivity	= 0.056 A/W
d	= the focal plane aperture diameter	= 0.45 mm or 4.5 mm
x	= the distance of the beamsplitter from the focal plane	= 0.75 m
η_{01}	= the optical efficiency in the path of the scattered light	= 0.5
$g(90^\circ)$	= the scatter coefficient in the direction of the aperture	~ 10^{-4} sr^{-1}

The backscatter current from the lens and all other optics in the path is given by:

$$i_{sc2} = \left(\frac{\pi r_c P d^2}{4}\right)\left(\frac{\eta_{02} g_2(180^\circ)}{f^2}\right) \qquad (2\text{-}42)$$

where:

f	= the focal length	= 1.5 m

$g_2(180^o)$ = the composite scatter function from lens and other optics $\sim 2 \times 10^{-3}$ sr^{-1}

η_{02} = the transmission of the optics including the beamsplitter = 0.1125

So the optics scatter current is:

$$i_{sc} = \frac{\pi r_c P d^2}{4}\left(\frac{\eta_{01} g_1(90^o)}{x^2} + \frac{\eta_{02} g_2(180^o)}{f^2}\right) \qquad (2\text{-}43)$$

By substitution of the values:

$i_{sc} = 4.2 \times 10^{-7}$ A for d = 0.45 mm

$= 4.2 \times 10^{-5}$ A for d = 4.5 mm

With the 100/1 beamsplitter in the path, the current with the small aperture is not sufficient to cause saturation, but the current with the large aperture will still saturate the denominator PM. Therefore, some modification is again necessary. The calculations show that the contribution from the 50/50 beamsplitter is comparable to the contribution from the lens and other optics.

The selection of values for the scatter coefficients is critical and deserves further explanation. The scatter coefficient at an angle θ is given by:

$$g(\theta) = \left(\frac{a(\theta)}{4\pi}\right) S \qquad (2\text{-}44)$$

where:

S = the fraction of the incident light scattered

$a(\theta)$ = an anisotropic scattering function, defined here as the level of scatter intensity at angle θ relative to an isotropic scatterer.

For the beamsplitter which is in an enclosed area, the total fraction of light scattered from the two surfaces is typically between 0.1 and 1 percent, say 0.25 percent. The anisotropy function reaches a minimum around 90 degrees as shown by the measurements of different researchers; a value of 0.5 is assumed. Thus:

$$g_1(90^o) \sim \frac{.5}{4 \times 3.14} \times 2.5 \times 10^{-3} = 10^{-4} \text{ sr}^{-1} \qquad (2\text{-}45)$$

For the lens and other optics the breakdown of the contributions to $g_2(180^o)$ is as follows:

Component	S	$g_2(180^o)$
Lens	0.5%	0.2×10^{-3} sr^{-1}
Mirror	3.5%	1.4×10^{-3}
Light Trap	1%	$.4 \times 10^{-3}$
		$g_2(180^o) \sim 2 \times 10^{-3}$ sr^{-1}

An anisotropy value of 0.5 is assumed for each element. Fresnel reflections are not a factor because none of the optical surfaces with the exception of the lens center is perpendicular to the beam. If necessary, the lens center can be compensated by obscuring a small spot in the center of the beam.

2.2.2.3 Receiver Features for Accepting High Current Levels

The calculations have shown that conditions exist under which tube saturation can occur. For the most part, it appears that operation with the small aperture (the primary intent of the system) will not cause saturation of the denominator channel, even in the heavy fog condition ($\sigma = 0.035$ ft.$^{-1}$) with the use of a 100/1 beam-splitter. However, when the large aperture is inserted, saturation will occur. Therefore, for this reason (and also as a margin of safety in the small aperture case), the system has been designed with the capability to further ensure against saturation. The steps taken to handle the high initial atmospheric and optics backscatter are, therefore:

- Use two photomultipliers , one for the numerator measurement, and the other for the denominator.
- Insert a 100/1 beamsplitter before the PM tubes, the one percent going to the denominator. The attenuation of 100

in signal current is accounted for in the processor.

- Vary the photomultiplier gain. The system has the ability to gate the PM tubes "off", and then turn them "on" quickly (~ 100 nanoseconds). Therefore, if saturation conditions exist, one can wait until the signal return is below saturation before turning the PM tube on.
- Provide additional attenuators in the denominator PM path for the case of very heavy fogs and the large aperture. Again, the additional attenuation has to be compensated for in the processor.

The first two steps will always be taken. The third step (rapid turn-on of the PM tube) will generally be used. However, extensive testing of the system may ultimately indicate that saturation is not a problem in the small aperture condition, in which case the PM tubes might be left on. At this time, however, rapid turn-on of the PM tubes at the appropriate moment is seen as a standard operating procedure. The last step will require a great deal of field testing to determine the signal levels and atmospheric conditions which may have to be considered.

2.2.2.4 Required Amplifier Gain

Since conditions exist wherein PM tube saturation takes place, that (saturation) point must be the criteria for the electronic design. For a peak cathode current level of 10^{-8} ampere and a typical PM tube gain (for the 4516) of 8×10^5, the peak anode current in the denominator channel is:

$$i_{p-a} = i_{p-c} \times G = (10^{-8})(8 \times 10^5) = 8 \times 10^{-3} \text{ ampere} \quad (2\text{-}46)$$

Using a 50 ohm resistive load, the maximum output voltage is:

$$V_{max} = (8 \times 10^{-3})(50) = 0.4 \text{ Volt} \quad (2\text{-}47)$$

Thus, a current gain of 10 (20 dB) is sufficient to produce a 4 volt output, which is a satisfactory (and desirable) input level to

the ensuing electronics (integrators, etc.).

Similarly, if the denominator channel is at saturation level (10^{-8} amp) after having been attenuated by a factor of 100 by the receiver beamsplitter, then the current level going into the numerator channel would be 10^{-6} ampere, which would saturate the numerator PM tube if it were activated. Thus, the numerator tube in this set of circumstances should not be turned on until the signal level has reduced to 10^{-8}. That occurs when the transmittance (T) drops to 10% ($T^2 = 10^{-2}$). At that point, the signal levels are identical to those analyzed (10^{-8} amp) above, and again a 20 dB amplifier will produce a satisfactory working voltage for the ensuing electronics. Thus, under conditions of saturation (or near saturation) levels into the denominator, the operating procedure should be to assume a low transmittance value, say 2%, and to turn the numerator on at a time corresponding to the 2% range. One can then work backwards in range, as desired, as long as the 10% transmittance point is not violated. Under conditions where the denominator channel is not at near saturation, the time at which the numerator may be energized becomes progressively shorter, and the transmittance value correspondingly higher. The range for which a measurement is desired is inserted simply by dialing a thumbwheel on the processor's front panel.

SECTION 3

EQUIPMENT DESCRIPTION

3.1 SYSTEM CONFIGURATION

The systems considerations developed in Section 2 dictated the design of the LIDAR SVR Transmissometer developed under this program. The system consists of four major subsystems: optics; laser; receiver; and electronic processor. The system is housed in a mobile van to allow testing at virtually any field site, as desired.

A simplified block diagram of the system is shown in Figure 3-1, and operation is as follows:

1. A pulsed laser beam is projected from the end of the runway up the approach path. Laser pulse duration is of the order of 4×10^{-8} sec. Laser beam divergence is less than 3 mr. The optical system beam divergence is approximately 10^{-4} radian.

2. A coaxial optical system collects the backscattered light from the laser pulse as it propagates up at an elevated angle.

3. A pinhole aperture in the focal plane at the collecting lens modifies the throughput of the telescope system in such a way that the efficiency of the system is proportional to the square of the distance from the receiver to the scattering element throughout the range of interest (~1 km).

4. The scattered light transmitted by the pinhole aperture is converted by detectors to currents proportional to the product of the scattered light received at the aperture of the telescope and the square of the distance to the scattering point.

5. The current is integrated over two time periods. The first begins just as the laser pulse leaves the optics, and the second starts at the range to which the transmission is to be determined. Both continue until the current has degraded well below the peak value.

6. The ratio of the second integrated signal (numerator) to the first integrated signal (denominator) is taken electronically and then

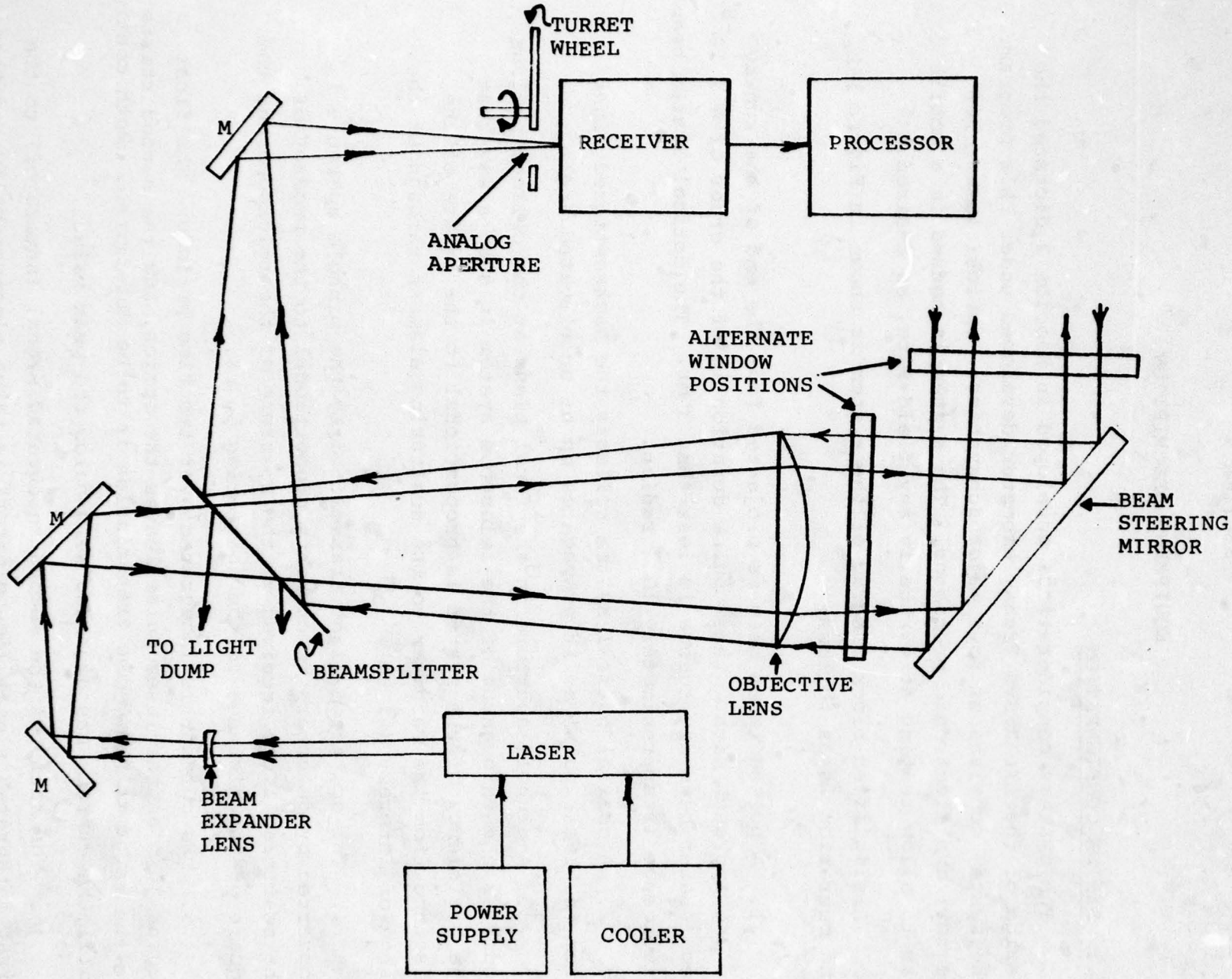

Figure 3-1. LIDAR System, Diagram

the square-root of this ratio is obtained electronically.

7. The value of the square-root so obtained is equal to the atmospheric transmission from the laser telescope system to the pre-selected point.

8. In the present system, the range can be changed manually on successive pulses, or every six seconds. It is clear that the transmission to several ranges could be measured simultaneously by integrating over several numerator time periods, if desired in an ultimate system.

3.2 OPTICAL SUBSYSTEM

The primary elements of the optical subsystem are as follows:

. Objective lens which both focuses the laser beam at a range of approximately 700 meters and focuses the backscattered radiation onto a focal plane aperture.

. Negative lens which forms the laser beam expander in combination with the objective lens.

. 50/50 beamsplitter which combines the beam and receiver into a coaxial unit.

. Light trap which absorbs the unused laser output passing through the 50/50 beamsplitter.

. Mirror which bends the transmissometer path to the direction of interest (beam-directing turret).

. Reference system at the turret wheel for checking alignment of the beam and receiver.

Mechanical arrangement of the elements is as shown in Figure 3-2. The entire mechanical structure depicted in Figure 3-2 is constructed of glass, and is shown in the photograph of Figure 3-3(a). Glass construction was chosen because of its low thermal coefficient of expansion. Temperature changes will result in wavefront aberrations, which will alter the focal position of the lens with respect to the position of the analog zone. Analyses have indicated that the wavefront aberration should not exceed $\lambda/4$, where λ is the wavelength.

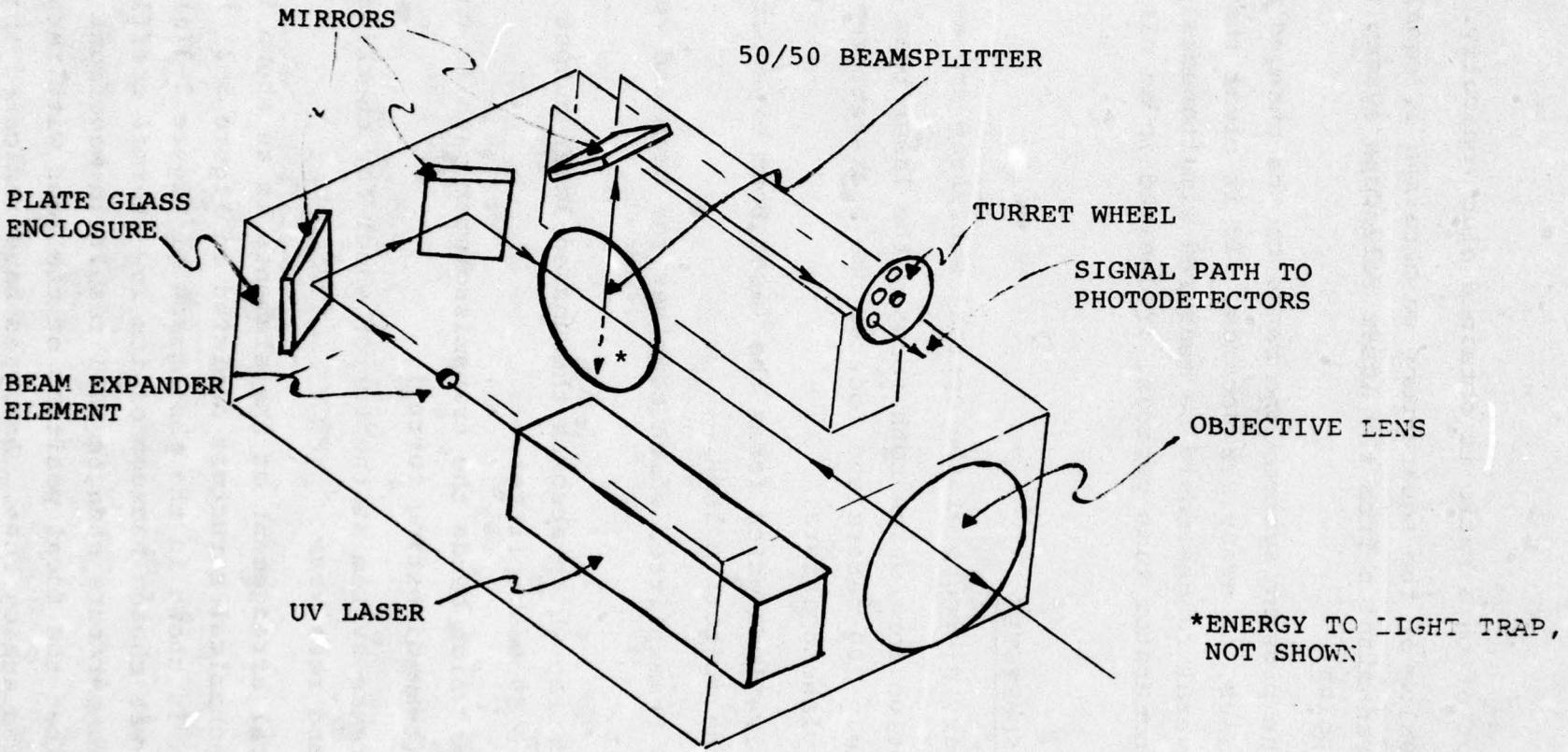

Figure 3-2. Mechanical Arrangement of Optical Components

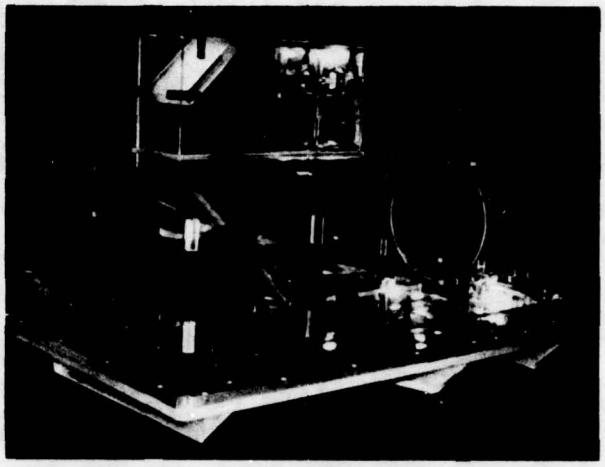

(a) Glass Construction

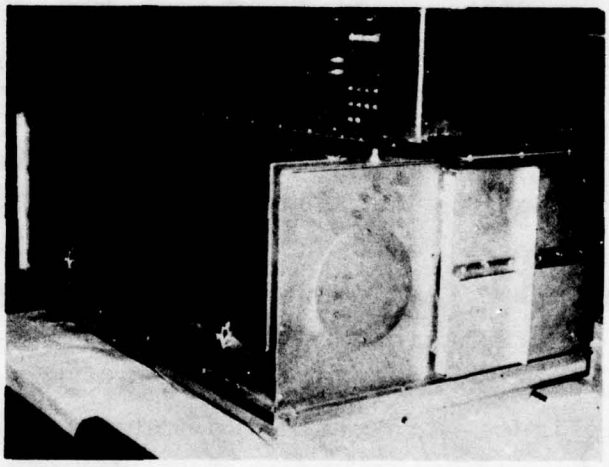

(b) System in Metal Enclosure

Figure 3-3. Mechanical Construction of LIDAR System

For this requirement, the studies showed that the use of glass would eliminate all temperature problems completely for a range of $\pm$ 5°C. By comparison, however, the use of aluminum would require temperature control of $\pm$ 0.6°C., a difficult problem in field use.

All of the glass elements are cemented together under controlled laboratory conditions. Less critical elements are mounted on smaller metal (KOVAR) plates, which are then cemented to the main elements at the appropriate places. The glass frame is also reinforced by other glass ribs to stiffen the structure. The entire unit is then housed in a metal enclosure for further protection, as shown in Figure 3-3(b).

With the stability of the receiver and transmitter optical trains thus assured, it is then only necessary to focus and align the laser beam within the appropriate analog zone. Only two adjustments then remain available to the operator to achieve the focus and alignment of the laser beam: (1) an axial motion of the laser-beam expander lens, and (2), transverse and angular motions of the laser itself which are accomplished by fine adjustment screws on the laser mount.

The requirement that the laser beam be confined within the analog zone out to a range R_b permits the quantification of the factors which tend to destroy optical performance of the system. Table 3-1 summarizes the error budgets established during the program for each of the major categories of effects which deteriorate performance. Here all error budgets have been converted to equivalent wavefront deviations in terms of the basic wavelength of 3471 Å. Wavefront deviations may be related to changes in sizes of images and to angular errors. Compliance with these individual error budgets is met by: (1) specifications on components; (2) machining and other fabrication tolerances; (3) suitable choice of fabrication materials; and (4) assembly techniques.

3.2.1 OPTICAL COMPONENTS

The objective lens has a diameter of 30 cm and a focal length of 150 cm. It is made of BK 7 glass and is plano-convex, having an aspheric surface on the convex side so as to correct for spherical aberration to within one wave.

Table 3-1. Breakdown of Performance Error Budgets

A. ANALOG ZONE SIZE AND SHAPE (8λ Error Budget)	
1. Quality of Optics	1λ (RMS)
2. Analog Hole Size	1λ
3. Stability of Focal Length	1/4 λ
4. Contribution to Alignment Stability	1λ
5. Accuracy of Focus	Balance
B. LASER BEAM SIZE AND SHAPE (5λ Error Budget)	
1. Laser Beam Divergence (≤3 mrad)	0λ
2. Quality of Optics	1λ (RMS)
3. Stability of Focal Length	1/4 λ
4. Contribution to Alignment Stability	1/2 λ
5. Accuracy of Focus	Balance
C. LASER BEAM ALIGNMENT (10λ Error Budget)	
1. Inherent Laser Stability (≤1 mrad)	3λ
2. Decentration of Analog Hole	1λ
3. Contribution to Alignment Stability	1λ
4. Innacuracy of Aiming	Balance
D. ALIGNMENT STABILITY (2 1/2λ Error Budget)	
1. Temperature Stability of Optics (±5 °C)	1/4λ
2. Structural Deformations	Balance

The negative lens of the laser beam expander has a focal length of 3 cm leading to a beam expander of 50 X. Since the laser beam has a diameter of approximately 5 mm, the expanded beam has a diameter of 25 cm. An additional lens is provided to focus the beam in close when the large (4.5 mm) focal plane aperture is used. As indicated earlier, two focal plane apertures are provided. The normal one has a diameter of 0.45 mm, and is satisfactory for the range of extinction coefficients of interest. The larger aperture is to be used only in heavy fogs. Both apertures are mounted in a turret wheel which is aligned such that one merely rotates the proper aperture into place.

The 50/50 beamsplitter is located on the image side of the objective lens rather than on the object side, which is the more normal case. This eliminates the need for a large lens in the laser beam expander, and reduces the beamsplitter size. Further, all dust is sealed out and scatter will only take place due to inherent imperfections on the beamsplitter. Since the beamsplitter is internal, however, it is operating in divergent light instead of parallel light. For a 45^{o} angle, astigmatism of the magnitude of 0.268t is introduced, where t is the thickness of the beamsplitter. To be acceptable, the thickness is held to .2 cm. The resultant beamsplitter has a major length of 8 inches.

Because the optical system is coaxial (i.e., the same objective lens is used for transmitting and receiving), a 50/50 beamsplitter (discussed above) is used to direct the energy to the proper places. That means that on transmission, half the laser energy is directed away from the transmission path, and is lost. However, one cannot allow that "lost" energy to scatter off internal system elements (fixtures, walls, etc.) and reflect back into the receiver, where this energy can either saturate the PM tubes, or be confused with the desired received signal. Therefore, a light "trap" must be utilized. Since the laser light is some 99% plane polarized, a very effective trap is made by placing a flint glass plate in the path of the reflected light at Brewster's angle. The angle of incidence cannot be exactly at Brewster's angle for all rays since we deal with a cone that has a half angle of 4.76^{o}. Those rays reflected by the flint

glass are then collected on a diffuse black surface. Calculations indicate that the resultant energy backscattered to the receiver from this light trap is much lower than the scatter expected from dust and scratches on the system's optical surfaces. A schematic of the light trap is shown in Figure 3-4(a) and a photograph is shown in Figure 3-4(b).

The remaining optical elements are simple; i.e., beam bending mirrors, output window, and beam directing mirror. All elements, with the exception of the negative element of the laser beam expander, are permanently bonded to the all-glass support structure. Those elements that are utilized for receiving, (i.e., objective lens, beamsplitter, folding mirror, and the indexed aperture wheel) are pre-aligned at the manufacturer's facility, and are designed to remain in correct alignment when operated at a test van ambient temperature of $20^{o}C \pm 5^{o}C$. The laser assembly, located within the optical assembly, has adjustable mounts to enable its output beam axis to be made co-incident with the output path pre-defined by the optical assembly.

The optical assembly is supported by a massive, shock mounted aluminum tooling plate, and is totally enclosed by a foam-rubber-lined aluminum enclosure.

3.3 LASER SUBSYSTEM

The laser sub-system is a frequency-doubled, Q-switched ruby laser, consisting of a water cooled laser head, Pockels cell Q-switch, second harmonic generator (SHG) crystal, and additional optical elements (i.e., dichroic filters and polarizing plates). Due to the complexity of the system, testing is performed in a sequential manner beginning with a basic, non-Q-switched ruby laser configuration and proceeding to the final configuration. In this manner, baseline performance data is taken in the various intermediate configurations as a means of establishing reference criteria, should any of the elements need to be replaced in the future.

The laser assembly (Figure 3-5) is mounted within the optical assembly on adjustable mounts, permanently bonded to the glass assembly. In its present configuration, no direct means is provided

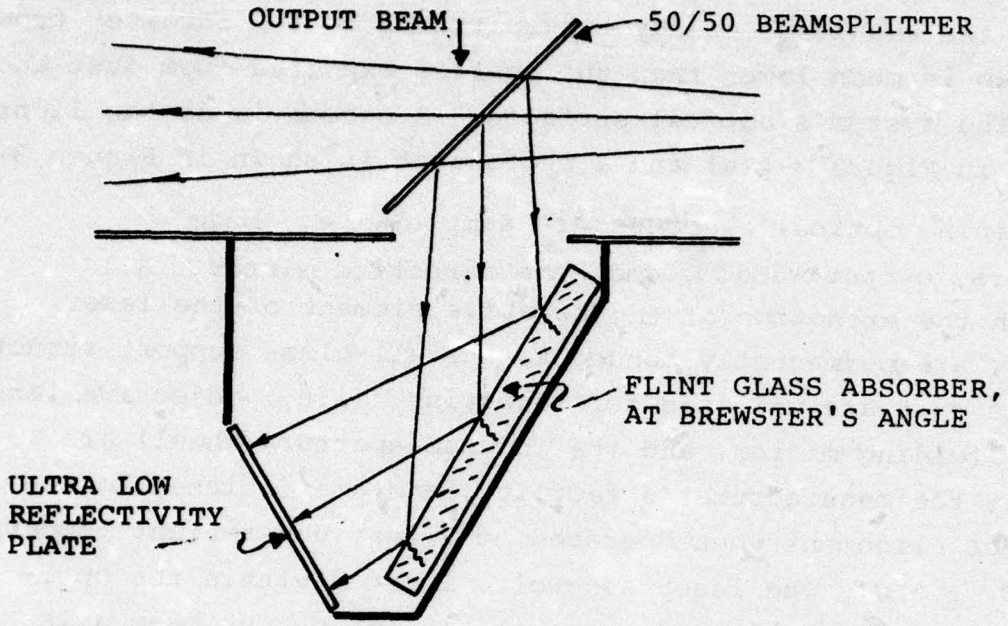

(a) Schematic, Light Trap

(b) Light Trap Assembly

Figure 3-4. Light Trap

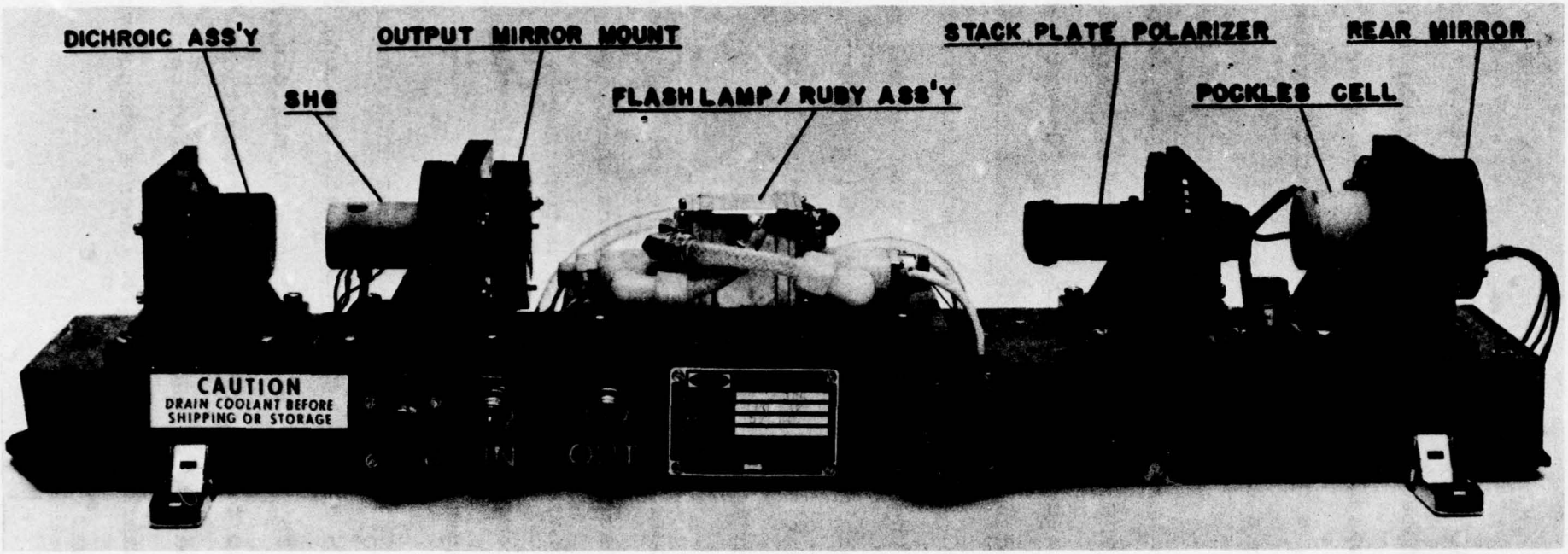

Figure 3-5. Pulsed U. V. Laser, Photograph

to monitor its operating characteristics, except for a PIN silicon photodiode (T_o detector), operating via a fiber optics bundle from 6943 Å (Ruby) leakage from the rear of the laser. With experience and familiarity, a qualitative assessment of system behaviour can be determined on a day-to-day basis.

Operationally, the basic Q-switched ruby laser can be activated as soon as the PFN capacitor bank is fully charged. A front panel switch on the laser HVPS permits either "Q-switched" or "normal" (long pulse) mode of operation for test and alignment purposes, but must be operated in the Q-switched" mode for frequency doubling in the SHG, since the energy density in the "normal mode" is well below the threshold required for doubling action in the SHG. The SHG component requires a 20 to 30 minute warmup to attain its proper operating temperature.

An access panel is provided in the optical assembly cover for access to the laser's rear mirror mount should any fine tuning of the laser be required. It must be noted, however, that should any of the laser's component parts require replacement, a complete laser and system realignment must be performed.

Laboratory testing of the laser was undertaken in a systematic manner, beginning with a very basic configuration, consisting of a flash-pumped ruby and the two resonator mirrors, then proceeding to Q-switched and frequency-doubled configurations (Figure 3-6). The output parameters of each of these configurations are intended as useful "benchmarks", should the laser's output characteristics degrade with time.

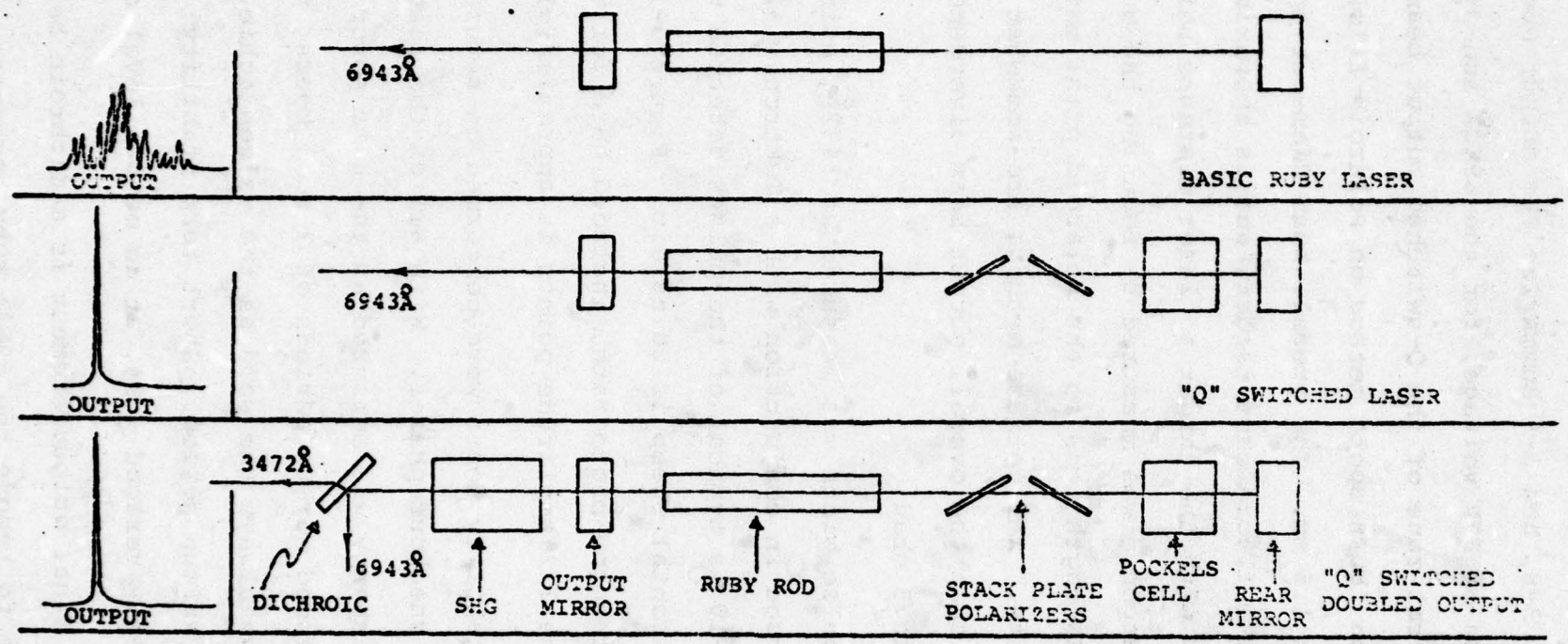

Figure 3-6. Laser Configurations

Figures 3-7, 3-8, and 3-9 summarize the output energy available as a function of PFN voltage, for the 6943Å and 3472Å wavelengths. The intense, central zone of the Q-switched output beam (as characterized by the common "burn spot" method on Polaroid film) is an oval, approximately 2 x 1.5 mm. The overall beam diameter appears circular, as viewed on a fluorescent target, and is approximately 5 to 6 mm in diameter, with the target to laser distance being about 1 meter. Beam divergence was measured by focusing the output through a 1.0 meter focal length lens to the Polaroid print material and fluorescing targets. While these methods are somewhat imprecise, it was concluded that the overall output beam divergence of the laser is less than 3 mrad.

The output pulse width was measured at 3472Å, using a Raytheon LA-31 detector, used in conjunction with a Tektronix 519 oscilloscope. Figure 3-10 is typical of the pulses detected with this system. The horizontal sweep is 20 ns/div. Figure 3-10 is a tracing of the oscilloscope photograph, included here for clarity. The pulse width at the 1/2 amplitude points is approximately 38 nanoseconds.

Amplitude stability tests were performed on several occasions during the final checkout phases. With all of the elements locked down, the output energy was measured at the same power supply settings. Over extended warmup periods of 2 to 3 hours, the output power measured was always the same as the values achieved after the 1/2 hour minimum warmup period. Short term stability; i.e., 40 - 50 consecutive pulses, averaged $\pm$ 9%, at an output level of 6.5 mJ.

The laser's final output element is a dichroic beamsplitter, whose function is to remove the 6943Å ruby component, and transmit

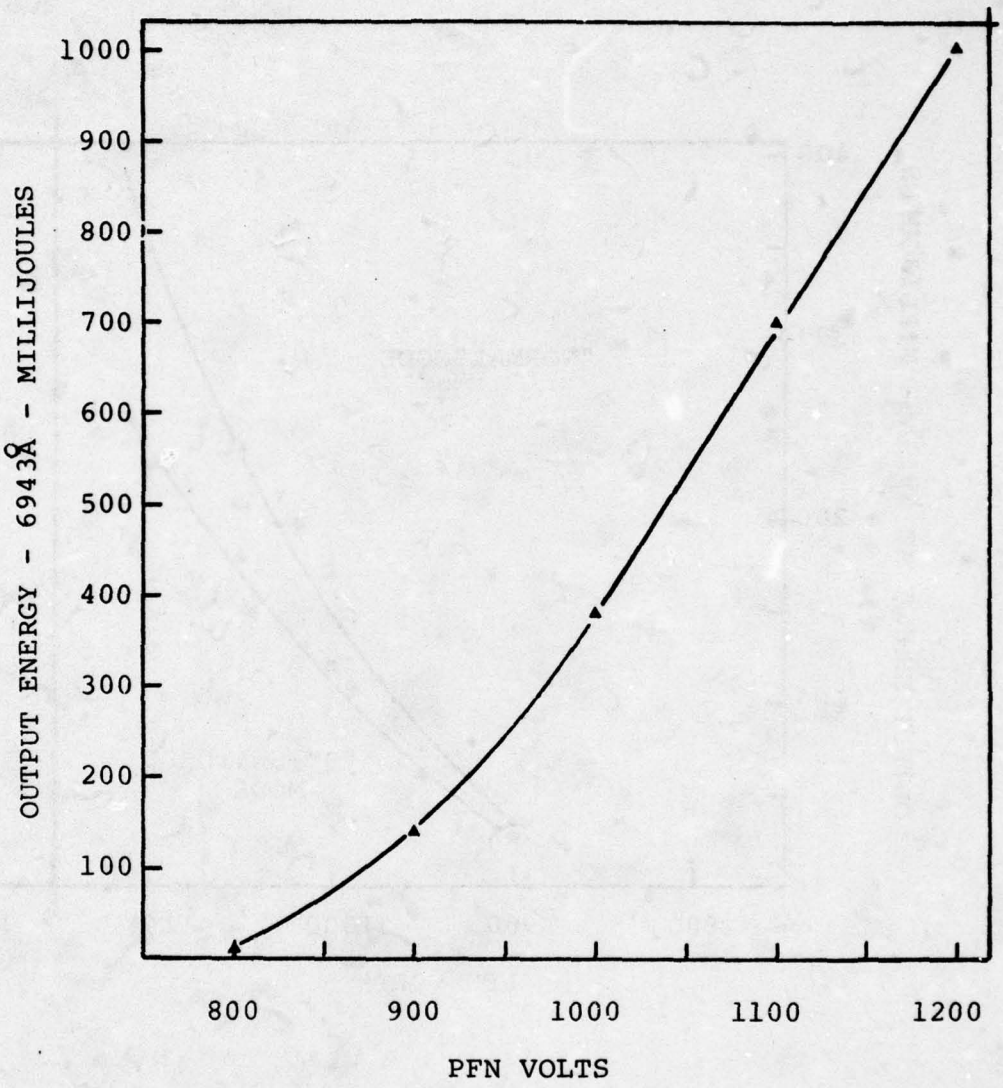

Figure 3-7. Basic Laser Output Characteristics
Non-Q-Switched Arrangement

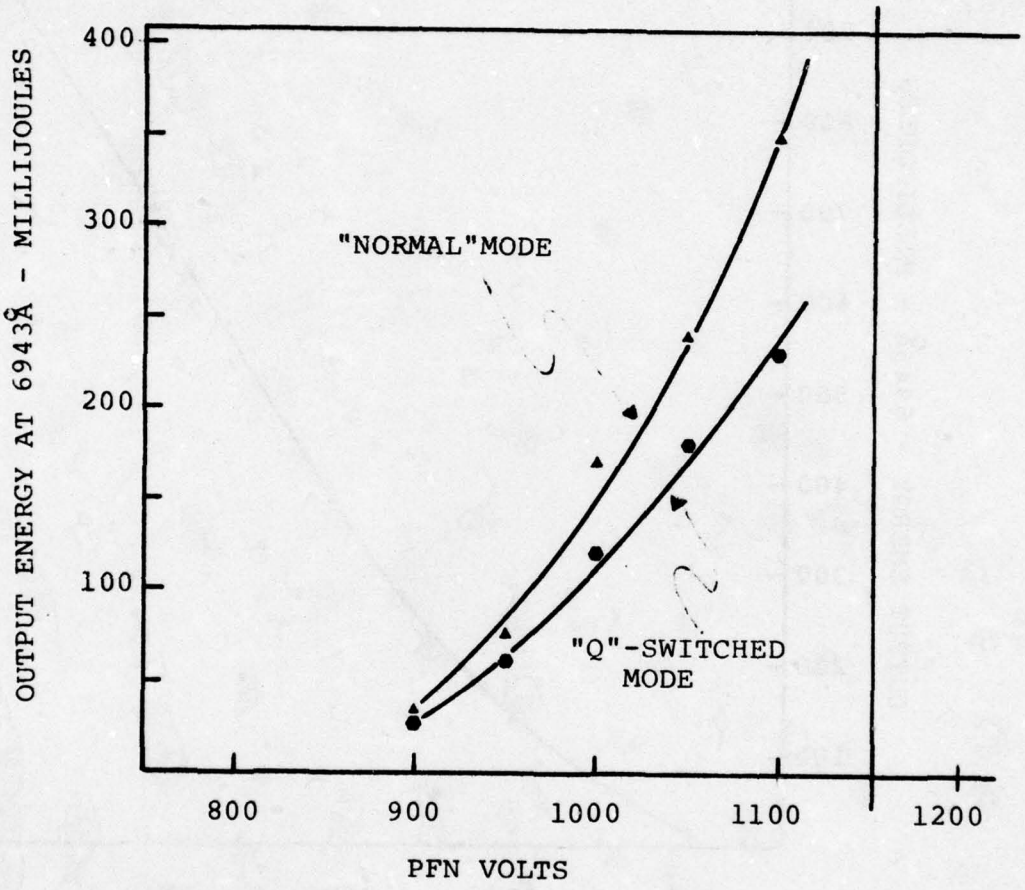

Figure 3-8. Laser Output at 6943Å in "Q"-Switched Configuration

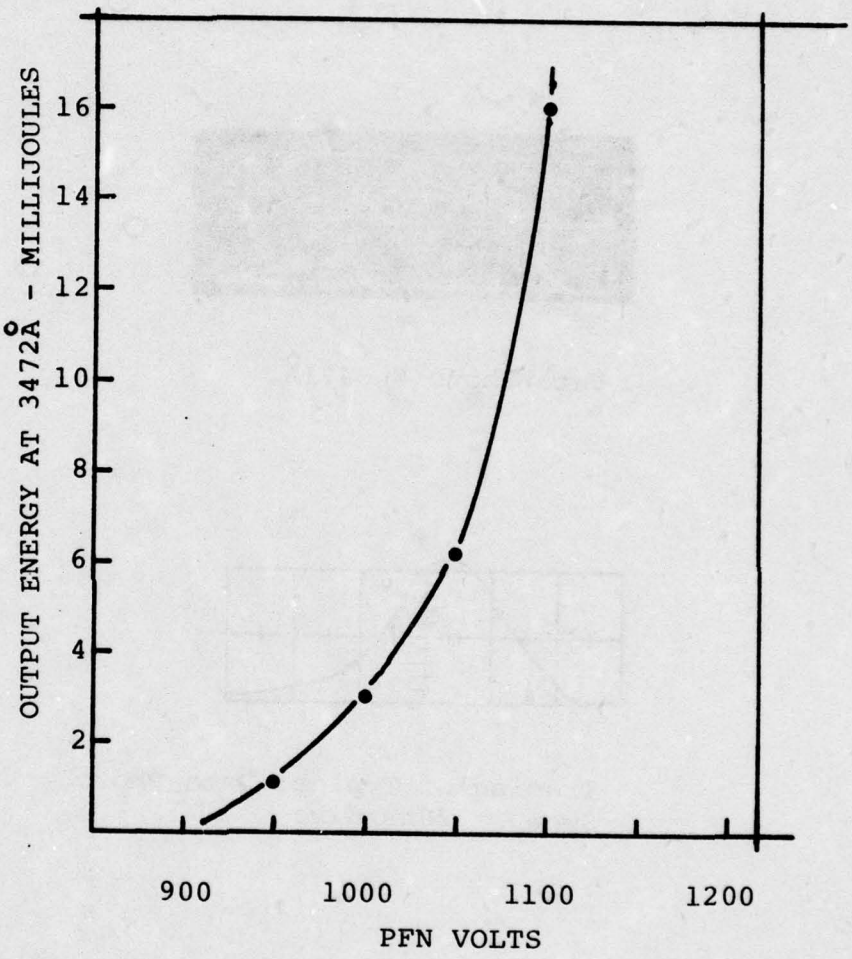

Figure 3-9. Frequency Doubled Output Characteristics

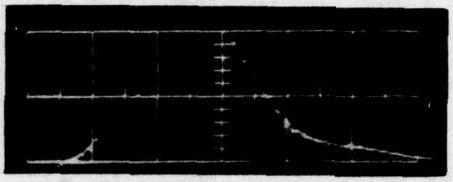

Data Photo @ 3471Å

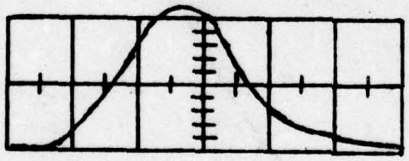

Tracing of Typical Data Photo
Sweep = 20ns/div.

Figure 3-10. Laser Pulse Width

the 3472Å U.V. line with minimum loss. Direct measurement of the 6943Å leakage was not possible with the instrumentation available. However, an indirect measurement was made by measuring the 6943Å beam with no dichroic in place and recording the oscilloscope deflection from the LA-31. The dichroic was inserted and the leakage deflection was measured. The following expression was then used to compute the estimated leakage:

$$E_L = E_O \frac{V_L}{V_O}$$

where:

E_L = Leakage energy

E_O = Energy with no dichroic

V_O = Voltage with no dichroic

V_L = Voltage with dichroic

Using typical output value for E_O (160 mJ)

$$E_L = 160 \text{ mJ } \frac{.02V}{15 \text{ V}} = .21 \text{ mJ}$$

3.4 RECEIVER SUBSYSTEM

The receiver subsystem is a self-contained unit, physically located on top of the optical assembly, consisting of the elements shown in Figure 3-11. Each element of the block diagram represents an individual module mounted separately with its connectors and power leads. Both the numerator and denominator channels of the LIDAR receiver have been electronically configured to be essentially identical. Since the components of each channel are the same, a single set of spares can be utilized on either channel. The one common unit shared by both channels is the receiver timing and control module. The function of this circuitry is to provide various timing pulses to control the high voltage and radio frequency (RF) switches. Within the timing and control module each channel is isolated although the individual integrated circuits used to generate the control functions are of the same type for both channels.

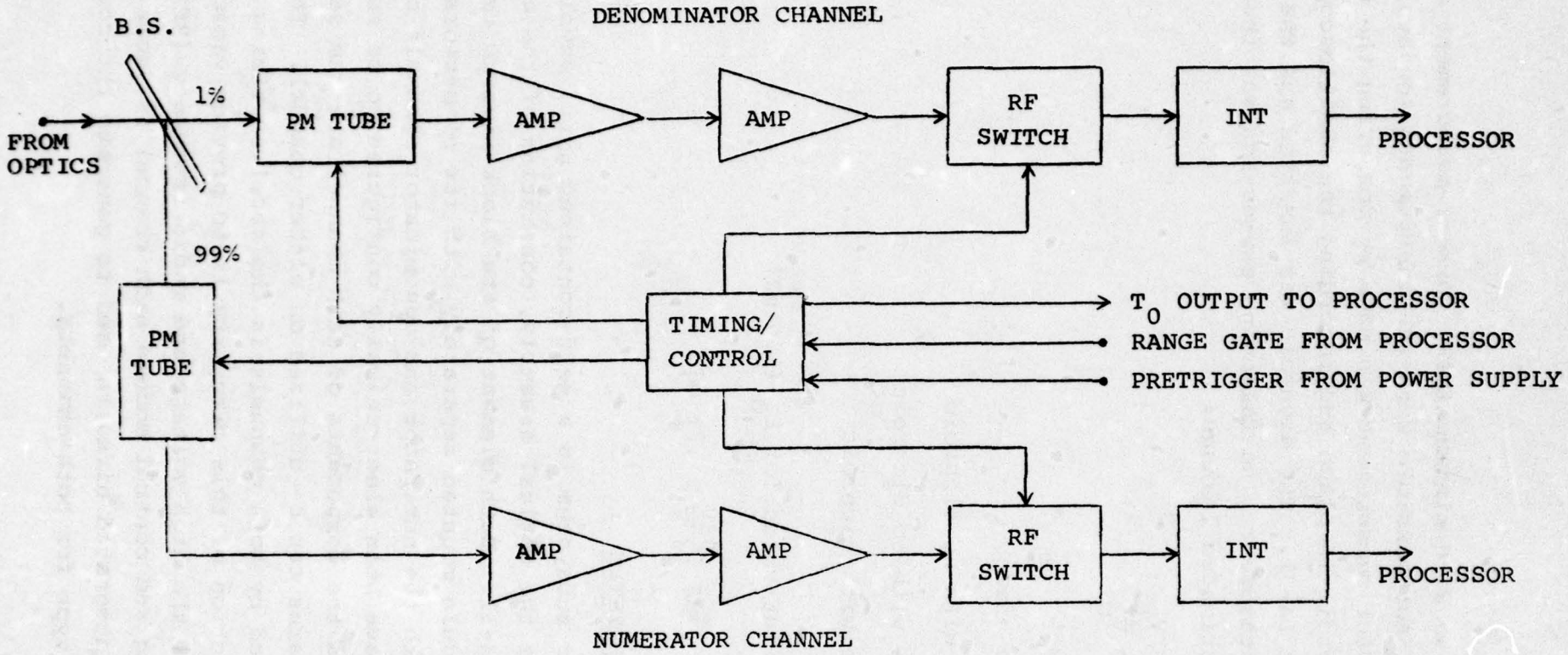

Figure 3-11. LIDAR Receiver Block Diagram

Following is a brief description of the signal path through the receiver. The backscattered signal photons enter the input to the receiver via the optical system's analog aperture. Photons are then directed to two separate but identical photomultiplier tubes by means of a 99 to 1 beamsplitter, the higher energy being reflected to the numerator channel. The PM tubes are individually gated with rapid turn-on characteristics, and the output of each is amplified by a total of 20 dB. At the input to the integrator is an RF switch also capable of fast turn-on. Signal currents are integrated over two time intervals; the first (denominator channel) begins as the laser pulse is propagated, whereas the second interval (numerator channel) occurs at the range selected by the thumbwheel switch located at the LIDAR signal processor. Both channels are switched off simultaneously at a time equivalent to the maximum propagation distance where accurate parameters are known. Since the transmitter optics are focused at about 700 meters, this would be the maximum distance where the analog zone data is valid, which is equivalent in time to approximately 4.7 microseconds. Integrator outputs are fed through coax lines to the equipment rack containing the LIDAR signal processor for final data analysis and display.

Referring to the block diagram of Figure 3-11, a more detailed description of each of the modules is presented.

3.4.1 PHOTOMULTIPLIERS

The RCA-4516 photomultiplier tubes are mounted within this light-tight assembly, together with their dynode networks. Also included as part of the dynode chain is a gain control circuit. This circuit is implemented by a dynode switching element in the form of a specialized high speed, high voltage transistor. The transistor circuit is placed between the first two dynode stages where the gain is the highest in the chain. The first dynode is held off from its normal higher bias voltage by the non-conducting transistor. During this time, the first dynode is biased at the lower potential of the second dynode, resulting in no gain between the two stages, thus greatly reducing the overall gain of the PM tube. Upon receiving a pulse from the timing module, the transistor

conducts, which then allows the first dynode to assume a higher potential to provide for full gain operation of the PM tube for the duration of the control pulse. Functional laboratory testing was undertaken prior to integrating the switching circuit as part of the PM assembly to determine the optimum transistor device and biasing conditions. The photographs of Figure 3-12 indicate the performance that was achieved with the finalized version of the PM switching circuit. As can be seen from photograph (B), full gain PM tube operation occurs at 150 nanoseconds after the control pulse is initiated. The first 100 nanoseconds is the total delay time of associated driver circuits while the remaining 50 nanoseconds is the actual turn-on time of the PM tube. The first 100 nanoseconds can be anticipated within the timing control system.

3.4.2 HIGH VOLTAGE POWER SUPPLIES

Each PM tube has its own independent high voltage supply. The supply is a fully encapsulated, modular DC to DC converter, operating from an input voltage of 24 volts. The output voltage is limited by a fixed resistor in series with an outside, panel-mounted, remote-programming potentiometer. This arrangement allows for fine resolution adjustment of the PM operating voltage so as to equalize the gain in each tube while protecting the tube from an overvoltage condition. Output ripple is 0.3% maximum at full load. This figure is significantly reduced at lighter load currents. Such is the case with the RCA-4516 PM tube.

3.4.3 AMPLIFIERS

There are a total of four, 10 dB gain amplifiers in the receiver, two for each channel. All of the amplifiers are identical and were selected because of their wide dynamic range and very low intermodulation distortion. With such characteristics, the amplifier is less likely to become saturated if the input stage is subjected to a high amplitude, transient-type of signal. These amplifiers achieve a low noise figure, flat frequency response, and linear phase characteristic with a high degree of gain stabilization

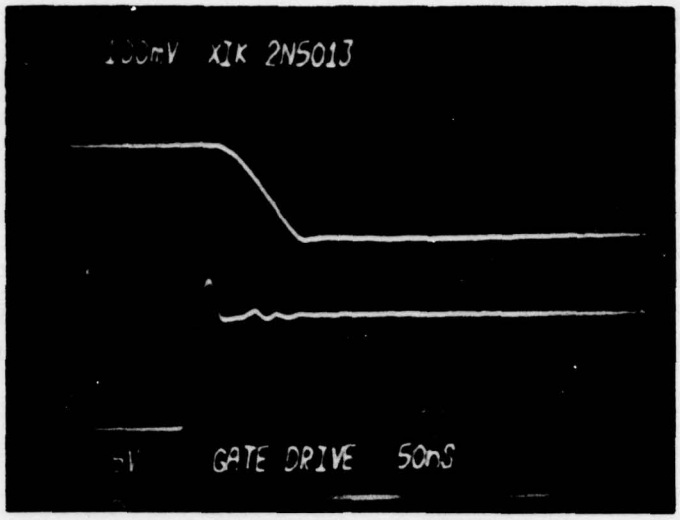

(A) Upper Trace: HV Transistor (Collector)
Lower Trace: Driver Circuit (Base)

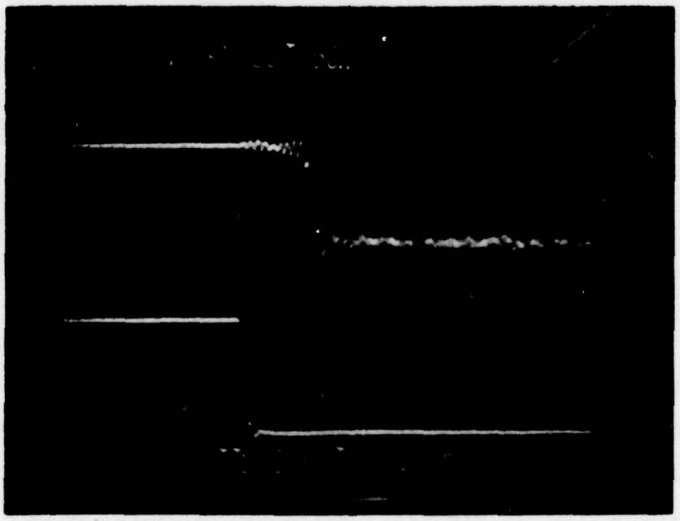

(B) Upper Trace: PM Tube Output (LED Source)
Lower Trace: TTL Control Gate Input

Figure 3-12. High Voltage PM Switch

from a unique, lossless feedback circuit. Maximum output capability of the device is +30 dBm, or 7 volts into 50 ohms.

3.4.4 RF SWITCH

The LIDAR system's return signal energy, after being detected by the PM tube and amplified, is directed to the integrators by means of a high speed, hybrid-circuit analog gate. The purpose of this switch is to prevent optical energy initially backscattered from the system to charge up the integrators as though an atmospheric signal had been detected. In the case of the numerator channel, the switch is kept open until a control pulse from the signal processor corresponding to the desired range is applied to the device. The unit is a SPST RF switch and driver stage contained in a single integrated circuit. Working directly from high speed TTL logic, maximum switching time has been measured to be less than 40 nanoseconds as seen in Figure 3-13.

3.4.5 TIMING AND CONTROL

The various timing and control pulses are developed within this module. The circuitry has considerable flexibility in that each of the output gates are independently variable relative to the time of laser pulse propagation, or T_0. A block diagram of the control function is shown in Figure 3-14.

The initial timing and control trigger pulse occurring at T_0 can be determined from either of two methods. From the laser power supply, a pre-trigger pulse is provided which is approximately 9 microseconds in advance of the actual laser pulse. Use of the power supply trigger allows us to anticipate the true T_0 and switch on the various active receiver elements slightly early should the cumulative turn-on times become excessive. This is accomplished by means of an adjustable delay stage, which can also be set to coincide exactly with the actual laser firing if so desired. The accuracy of this method to determine the instant of laser firing is limited, however, by any jitter or variation in the timing of the pre-trigger pulse. Jitter of the pre-trigger

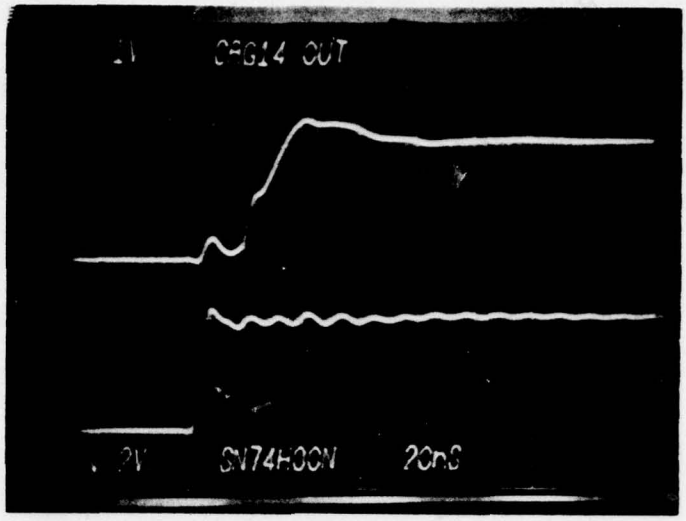

(A) TURN-ON TIME

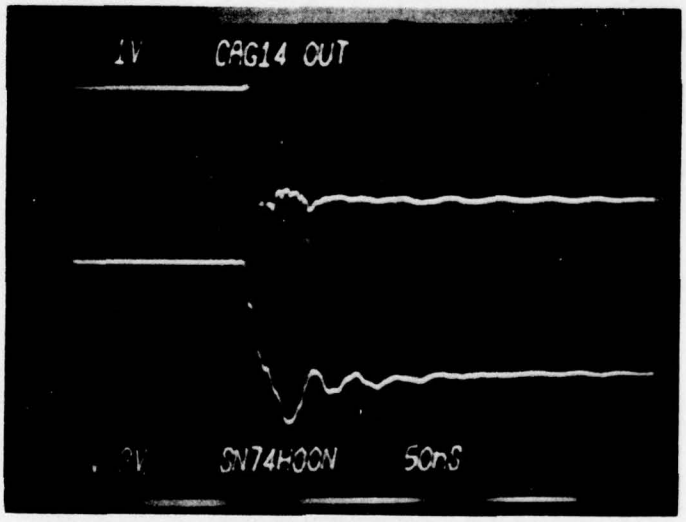

(B) TURN-OFF TIME

Figure 3-13. RF Switch Response
Upper Trace: Device Under Test
Lower Trace: TTL Gate Input

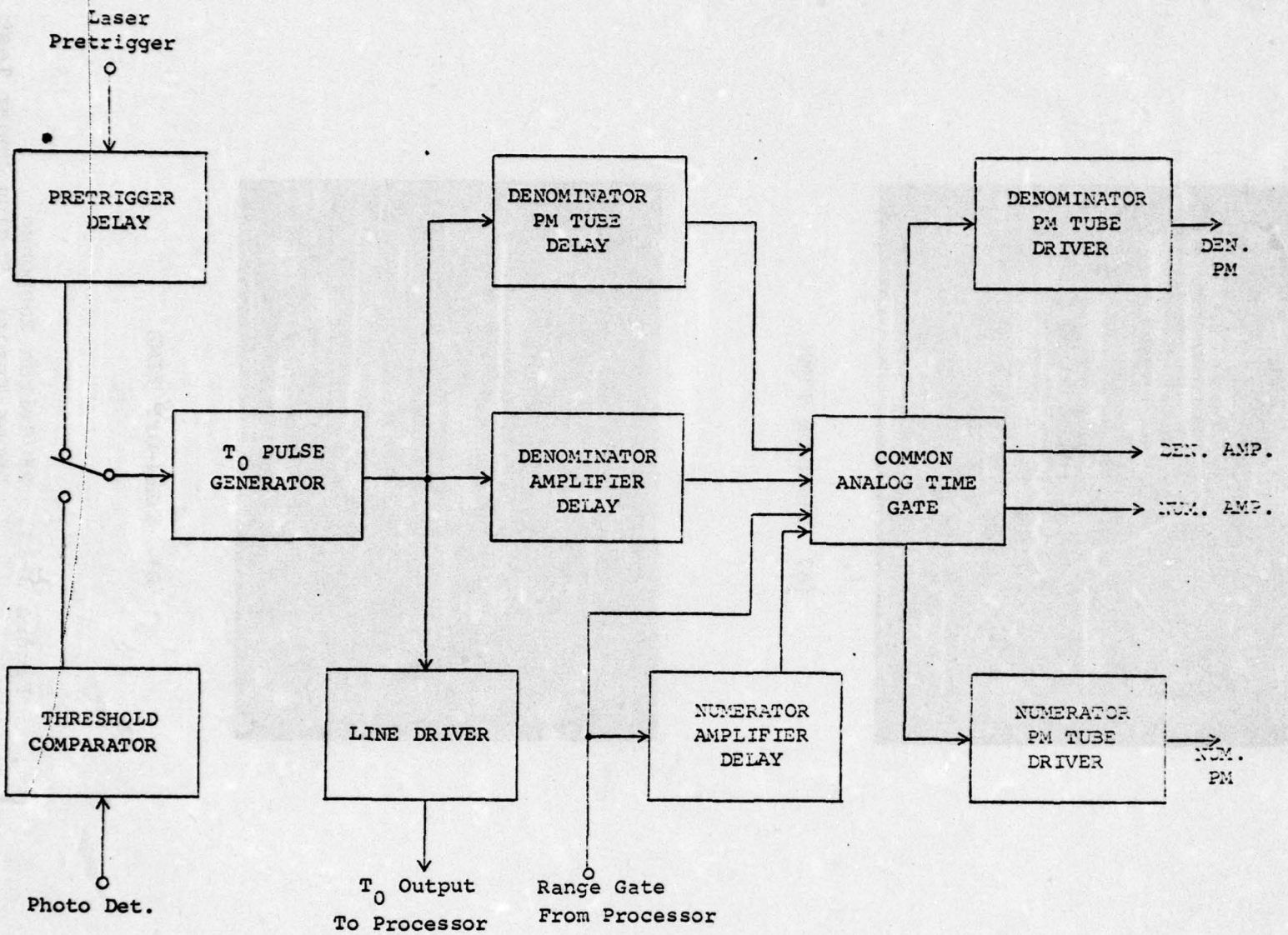

Figure 3-14. Timing/Control Block Diagram

relative to actual laser firing has been measured in the laboratory and is less than $\pm$ 10 nanoseconds. (Figure 3-15)

A far more accurate method of determining T_0 is to utilize a photodetector mounted at the rear of the laser. The detector samples the visible wavelength flash of the ruby rod through a length of fiber optics. Since the detector output is subject to some amplitude variation from pulse to pulse, a comparator stage is used with a variable reference to act as a threshold detector. Selection of either method is by means of a toggle switch located at the top of the box.

With the development of a suitable logic-type pulse defining T_0, the remaining gates for the PM tubes and amplifier outputs can be accurately referenced to the actual laser firing. This same T_0 trigger pulse is supplied to the LIDAR signal processor, which in turn delivers a signal back to the timing and control module to activate the numerator channel at a time coinciding with the range of interest. Turn-on of the denominator PM tube is delayed slightly from T_0 to avoid the initial optical backscatter effects. In order to eliminate undesirable turn-on effects of the PM tubes which could introduce an error at the integrator, an adjustable delay is used to switch the amplifier output to the integrator. A common output gate is used to simultaneously end the timing period of all functions.

3.4.6 INTEGRATOR

Because of the necessity to integrate fast pulses of 40 nanoseconds for short periods of time, about 6 microseconds, a simple RC integrator was chosen. To insure operation in the linear region of the integrator, a time constant 100 times longer than the integration time (100 x 6 μsec = 600 μsec.) was selected. However, the voltage output of an integrator of this type is very low. For instance, a step input to the integrator results in an output that will only grow to 0.01 of the input value in a time of about 0.01 time constants. This requires that an amplifier must follow the integrator. The amplifier need not be especially fast or have a high slew rate but should have low input offset

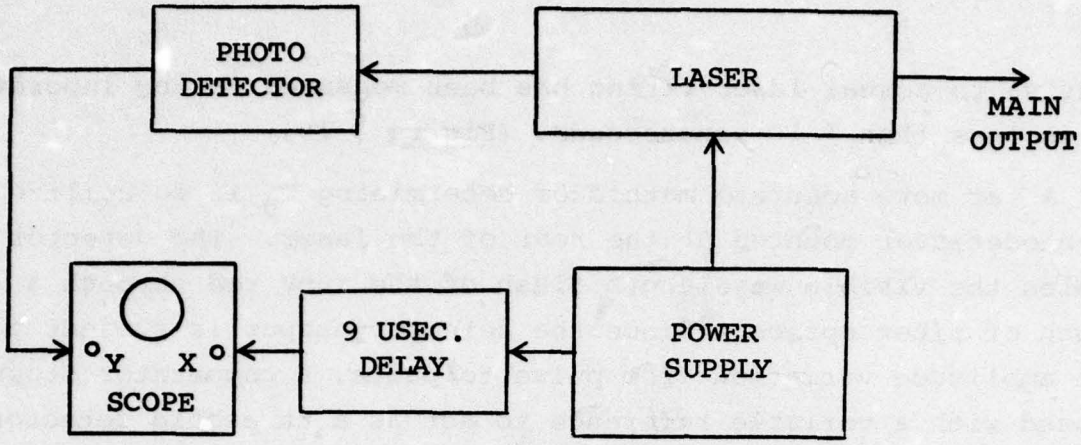

(A) Experiment For Observing Jitter.

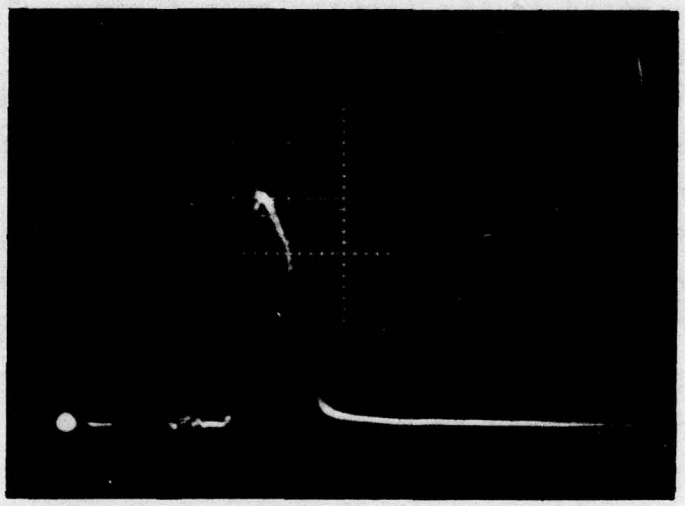

(B) Average Of 10 Consecutive Pulses
X-Axis: 100 Nanosec/Div
Y-Axis: 2 Volts / Div

Figure 3-15. Laser Power Supply Pretrigger

currents. An integrated circuit operational amplifier with a gain of ten is used to amplify the integrated signal information for transmission to the LIDAR processor.

3.5 PROCESSOR SUBSYSTEM

The LIDAR signal processor performs the final data analysis and provides the system output in the form of a digital display indicating a ratio proportional to transmissivity. The unit is contained in a standard EIA rack format (19" x 8.75" x 24") drawer mounted on slides within the equipment cabinet. A photograph of the complete assembly appears in Figure 3-16. In addition to the components required for processing, all of the system's low voltage DC power supplies are also mounted inside the drawer. Necessary DC voltages are distributed from the processor unit to the receiver subsystem located at the optics assembly.

In order to reduce the dynamic range requirements of the photomultiplier tubes, a two-channel system has been utilized. One channel processes that part of the signal that is the denominator of the transmissivity algorithm, and the other channel processes the numerator portion. The block diagram of the electronic signal processor is shown in Figure 3-17.

After the atmospheric return signal energy has been integrated, it is introduced to the processor by means of a sample-and-hold circuit. This sample-and-hold circuit (S/H) must have a very fast acquisition time (commonly known as aperture time) and must also hold the sampled information long enough for the log ratio module to settle down. A fast aperture time and a slow drift rate are opposing characteristics of a S/H, since a small sampling capacitor will permit a fast aperture time, but current leakage will cause the voltage to change rapidly. To circumvent this problem, a two-stage S/H has been employed. The first stage is a fast S/H whose output is followed by a slow S/H.

Recently, special functional modules have been developed that perform the computation $(X/Y)^m$, where m is controlled by a simple

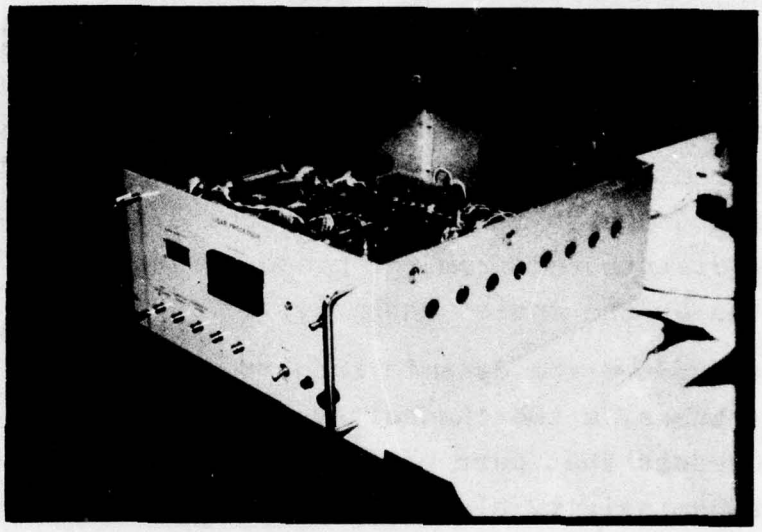

Figure 3-16. LIDAR Signal Processor, Photograph

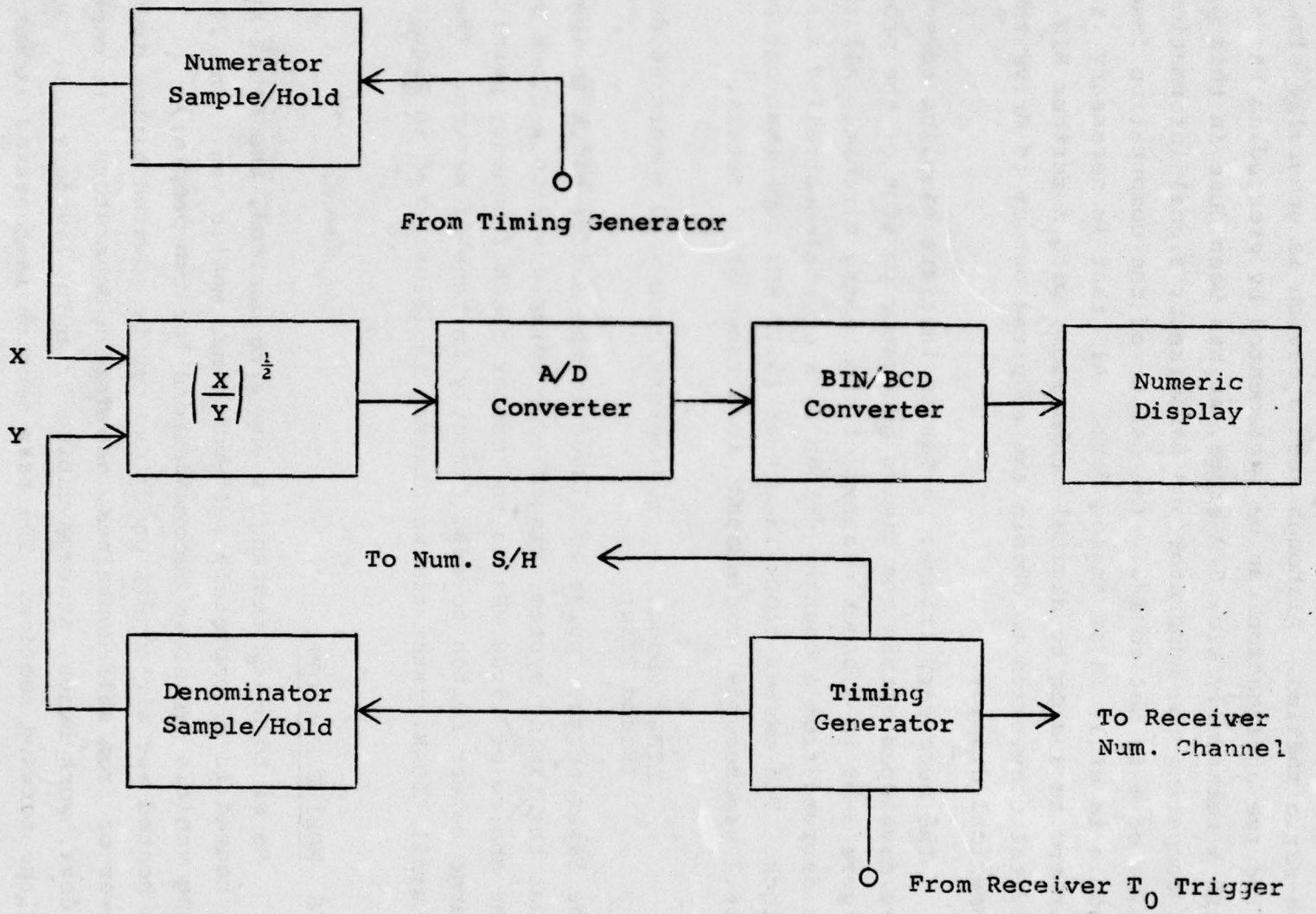

Figure 3-17. LIDAR Signal Processor, Block Diagram

resistive network. These devices are commonly referred to as log-ratio modules. Although such a device is generally slow, an effective utilization can be implemented by preceeding the module with a relatively slow S/H stage, as has been done in this processor. In comparing the numerator and denominator signal information, the value of m is set to 1/2. The output of the computation function module is still in an analog form. All that is necessary is to perform an analog to digital conversion, with a further BIN to BCD digital conversion to obtain the required output to drive the numerical display.

The necessary trigger pulses to initiate sampling commands are developed within the timing generator portion of the processor. Figure 3-18 is a block diagram of the timing circuit. All timing is derived from a counter driven by a crystal-controlled master clock. The master clock is set at 15.00 MHz such that one period (66.7 nanoseconds) corresponds to a range of 10 meters.

$$\text{LIDAR Range (Round Trip)} = 150 \text{ meters}/\mu\text{sec} = 10 \text{ meters}/66.667 \text{ nsec}$$

The laser trigger pulse is slaved to the master clock to insure that the timing system trigger edge coincides with a clock edge. The choice of 15.00 MHz as the master clock frequency permits the range select switch to read directly in tens of meters. The overall LIDAR system timing diagram is illustrated in Figure 3-19.

3.6 MOBILE STATION

So as to allow testing at any site desired, the LIDAR system is housed in a completely self-contained mobile van. The 27-foot long vehicle has sleep accommodations for two people; is heated and air-conditioned; and can be powered either from line power or from self-contained, gas-driven generators. It contains a desk, work bench, storage cabinets, and a lavatory, all located in the forward section. The rear section is reserved exclusively for the LIDAR equipment and allows ample room for moving about the system during operation. The interior layout of the van is shown in Figure 3-20.

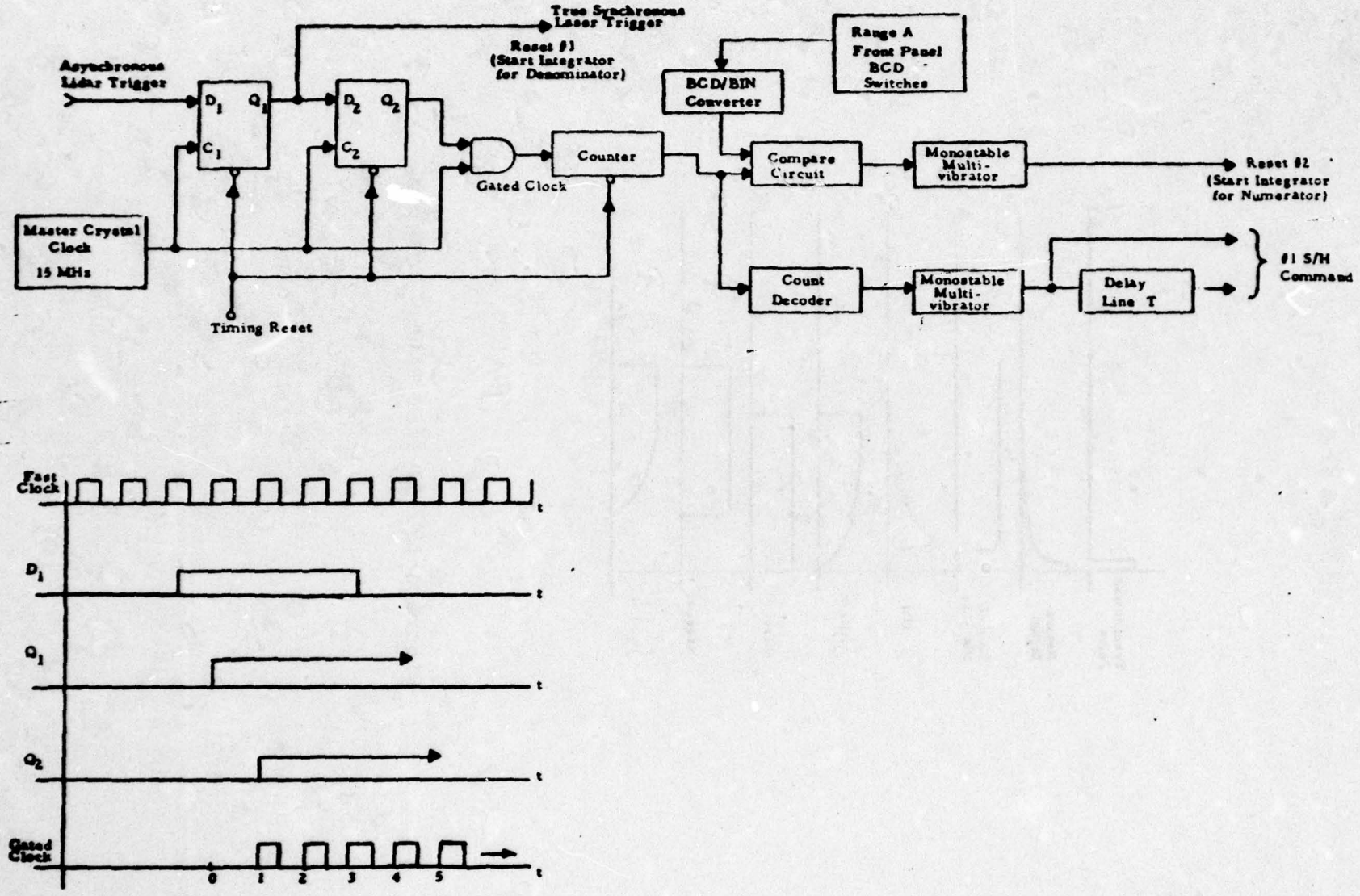

Figure 3-18. Timing Block Diagram

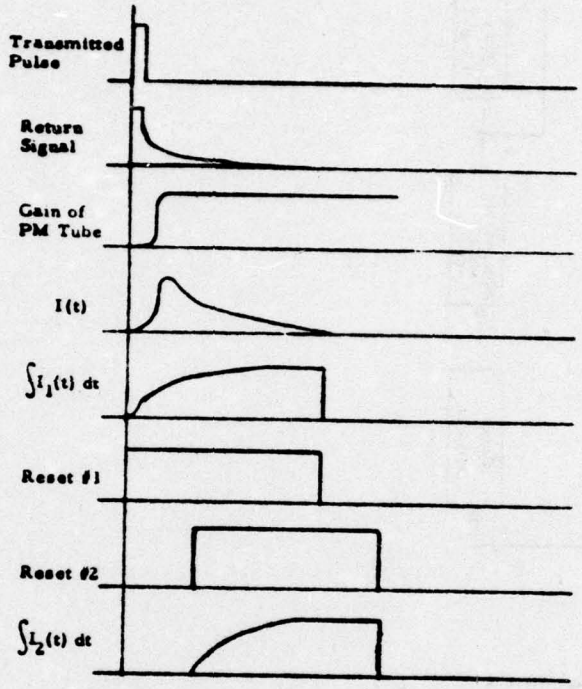

Figure 3-19. System Timing Diagram

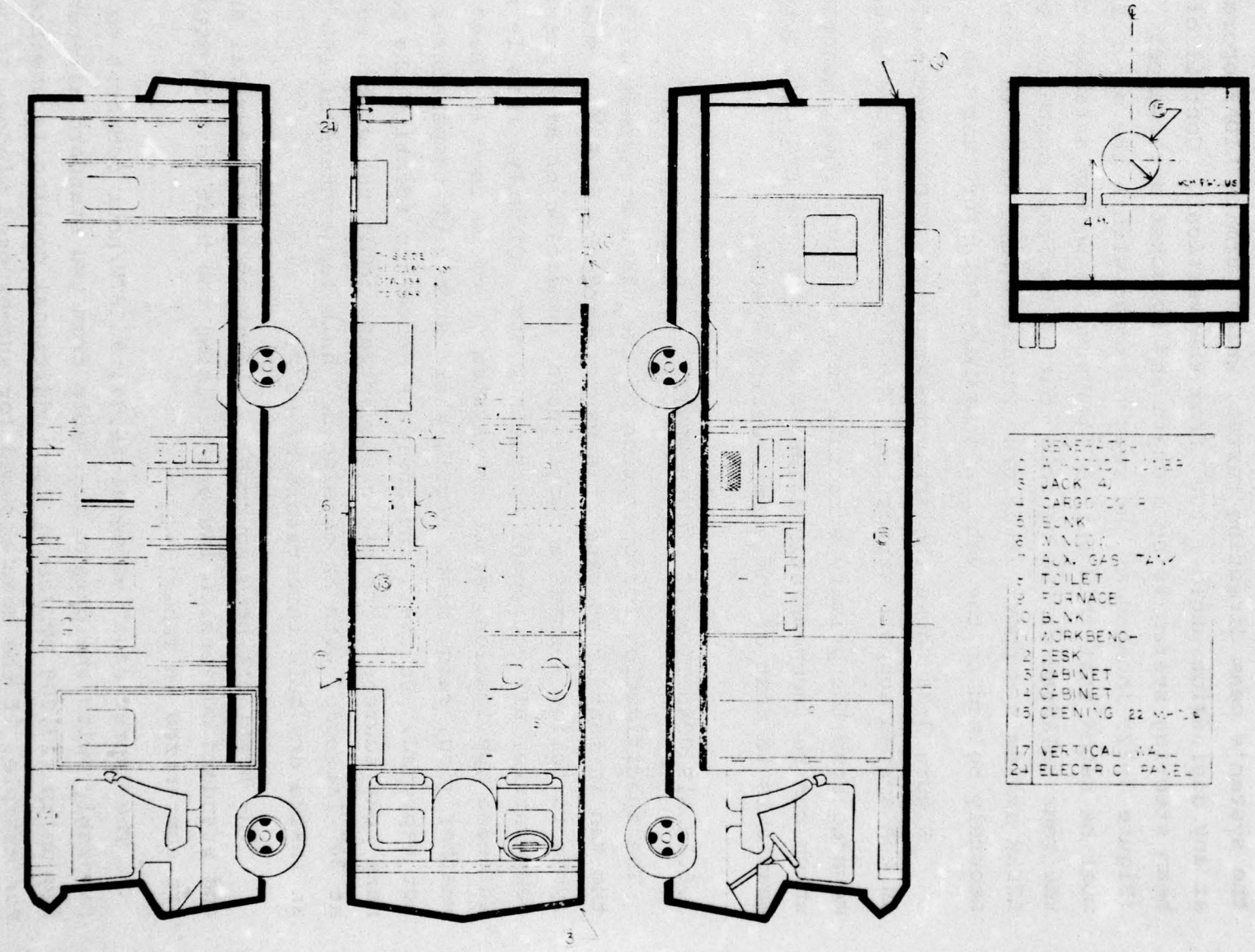

Figure 3-20. LIDAR Mobile Van Layout

The rear of the test vehicle (Figure 3-21) is dominated by the system's beam directing turret, which permits LIDAR operation at any depression angle $\pm$ 100° from the vertical. Control of this beam steering system is by a chain and sprocket arrangement (Figure 3-22) located at the rear bulkhead within the van. It must be noted that this entire subsystem in no way attaches to the rear bulkhead of the vehicle, but is entirely supported by the LIDAR system's support structure (Figure 3-23), which in turn, is securely bolted to the vehicle's primary structure through the floor.

Figure 3-24 shows the arrangement of the LIDAR system elements on the system support structure. The E/O components are independently mounted atop the primary structure on a massive, shock-mounted frame, which can be independently adjusted to match the system's output beam axis to that of the beam steering system.

3.6.1 AIR CONDITIONING REQUIREMENTS

The specification for operation of the LIDAR equipment within the van is that it operate at a van temperature of 90°F. The analysis to follow assumes a "worst-case" condition of high external temperature, all equipment operating, etc. Clearly, this is not the intended application, since the system is to be used in "bad" weather (fog, rain, mist, etc.), where such high temperatures are not expected. However, the analysis serves to identify the pertinent heat sources. The basic assumptions imply use of the equipment at 30° latitude, with an outside dry bulb temperature of 100°F., and an inside dry bulb temperature of 90°F.

The pertinent heat sources, in terms of their physical area, and standard conversion factors yielding the heat load in BTU/hour, are summarized in Table 3-2.

The "worst-case" value of 28,771.93 BTU/hour compares so favorably with the output available from two standard air-conditioning units (27,000 BTU/hour) that additional cooling is unwarranted. For example, if the heat assumed for sun-exposed windows is eliminated (hardly expected in fog, mist, or rain), along with its associated latent heat and duct loss, the cooling requirement

(a) Side View

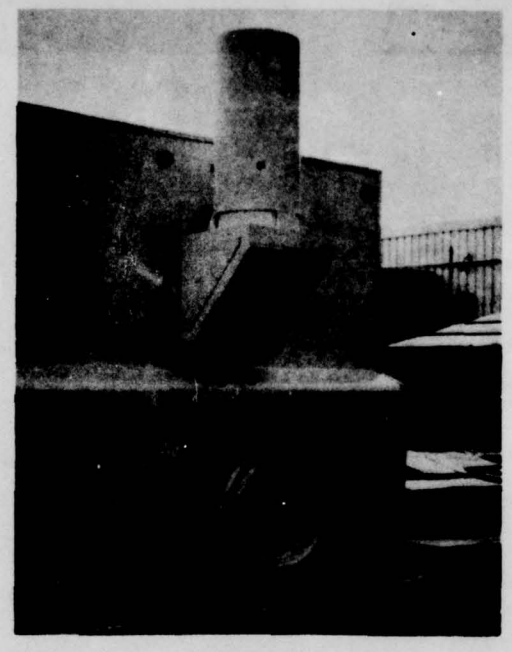

(b) Rear View

Figure 3-21. LIDAR Mobile Van, Photographs

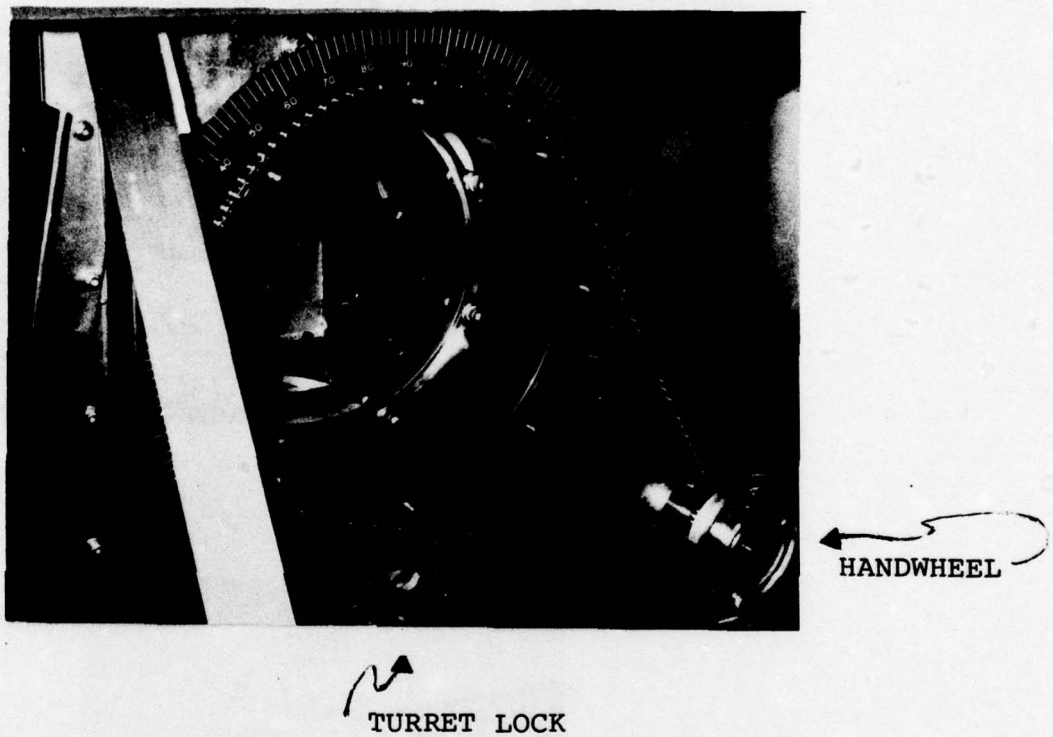

Figure 3-22. Beam Steering System

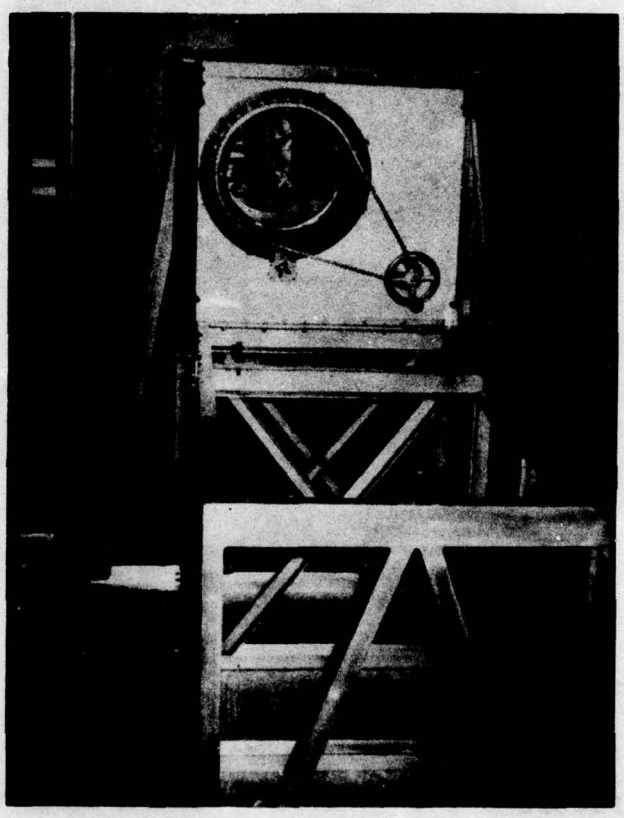

Figure 3-23. LIDAR Support Structure

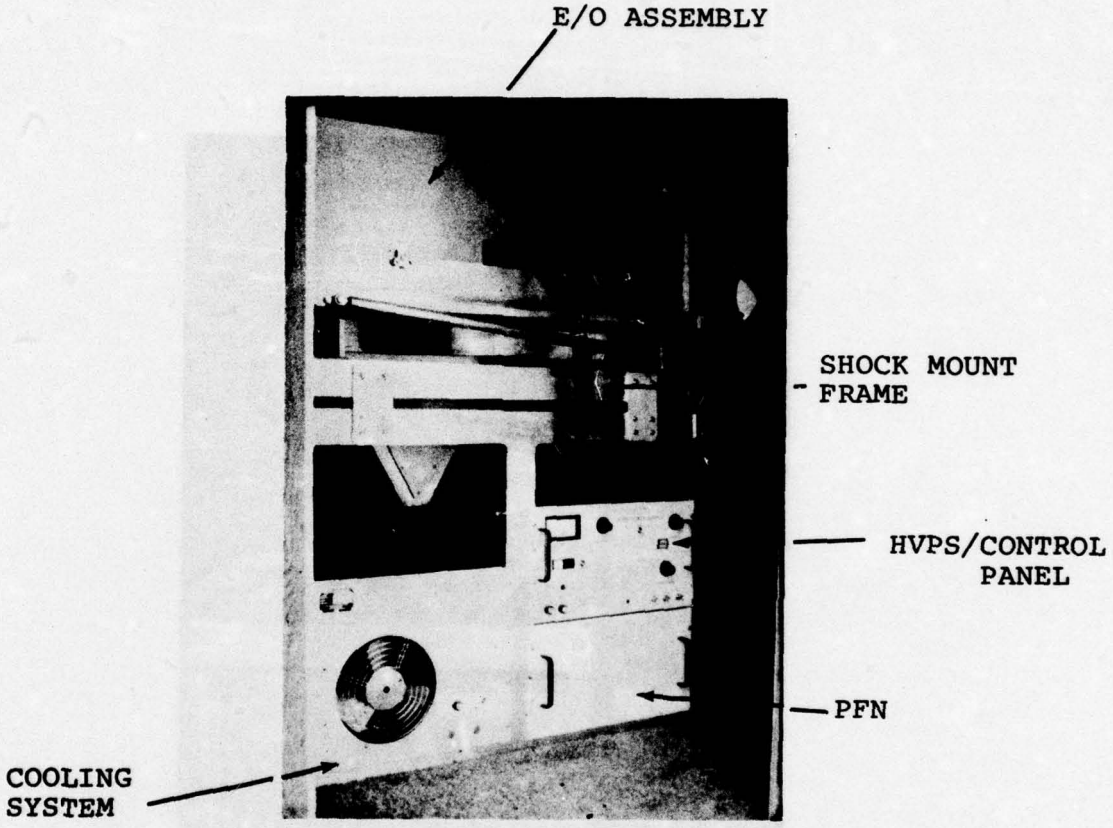

Figure 3-24. LIDAR System Arrangement in Support System

Table 3-2.

Worst Case Cooling Requirement

Item	Parameter	Multiplyer	BTU/Hr.
Sun-Exposed Windows (net)	12.10 sq. ft.	177	2141.70
Windows and Doors (gross)	69.99 sq. ft.	17	1189.83
Walls - Sun	410.66 sq. ft.	1.7	698.12
Shaded	54.36 sq. ft.	0.85	46.21
Ceiling	216.38 sq. ft.	4.4	952.07
Floor	216.38 sq. ft.	1.7	367.85
Volume (cu-ft)	1622.85 cu. ft.	0.18	292.11
Occupants	2	300	600
Equipment (watts)	4500 watts	3.4	15,300
Sub-total (sensible heat)			21,587.89
Latent Heat & Duct Loss		33%	7,124.04
Total Heat			28,711.93

drops immediately to 25,863.43 BTU/hour.

3.6.2 HEATING REQUIREMENTS

The cold-weather capability of the LIDAR equipment is specified as requiring operation at a van temperature of $45^{o}F$. An analysis similar to that of Section 3.6.1 was conducted with the prime assumptions of: outside temperature of $-30^{o}F$; a north prevailing wind; inside temperature of $45^{o}F$. The heat required is given simply by:

$$Q = \mu A \Delta T$$

where: μ = overall coefficient of heat transfer
A = area of heat transmission surface
ΔT = temperature difference = $75^{o}F$.

The pertinent sources of heat loss are calculated in Table 3-3:

Table 3-3.

Worst Case Heating Requirement

Item	Parameter	ΔT	μ	BTU/Hr.
Glass	69.99 sq. ft.	75	1.13	5,931.65
Walls	284.39 sq. ft.	75	0.12	2,559.51
Ceiling	216.38 sq. ft.	75	0.10	1,622.85
Floor	216.38 sq. ft.	75	0.34	5,517.69
Infiltration (1 vol/hr)	1622.85 sq. ft.	75/55	-	2,212.98
North Wall	180.63 sq. ft.	75	0.13	1,761.14
Sub-Total				19,605.82
Duct Loss (30%)				5,881.75
Total Heat Requirement				25,487.57

This "worst case" value of 25,487.57 is satisfied by a heating unit which provides 30,000 BTU/hour. Bear in mind also that the presence of 2 occupants plus operating equipment would also add heat, as given in Table 3-2, to further reduce the heating requirements.

3.6.3 VAN SPECIFICATIONS

The van purchased for this program is the Winnebago Model D-27S, customized as necessary. Pertinent vehicle statistics are as follow: Length: 27 ft. 2 in.; Width: 7 ft. 9 in.; Exterior Height: 10 ft. 1 in.; Interior Height: 6 ft. 6 in.; Chassis: Dodge M-500, 178 in. wheelbase, 14,500 lbs. GVW; Engine: 440 cu. inches, V-8; Transmission: 3-speed automatic; Steering: Power with tilt column; Brakes: Power with power front disc; Ignition: Electronic; Alternator: 60 Amp; Battery: Two 70 Amp-Hour; Tires: 8.19 x 5-D, 8 Ply front and dual rear.

The system includes two independent gasoline powered electrical generators. Each unit supplies 110 volt AC, 60 Hz., single phase with a capacity of 6500 watts. Total electric capacity available within the van is then 13,000 watts. The generators are shock-mounted on a sliding mechanism within a compartment accessible from the outside only. The compartments are insulated for thermal and noise considerations from the inside working area. Gasoline lines to supply the generators are installed from the fuel tank of the van. Control of (start/stop), performance monitoring, and output termination of each generator is placed within the power distribution panel. Necessary wiring for the output, wiring for measuring the accumulative running time, output voltage, and output current, and an on-off switch with a pilot light are provided to the distribution panel.

Two independent air-conditioning units are mounted on the roof of the van with required tubing and wiring. Each unit provides 13,500 BTU/hour capacity with separate thermostat control. Power source for these units is 110 volt AC, 60 Hz., single phase.

Each of the four corners of the van has a built-in hydraulic jack to enable leveling the van when parked on uneven ground. The

jacks are electrically controlled from within the van.

An extra wide door approximately 63 inches high by 37 inches wide is provided for loading and unloading equipment. An overhead drop-down bed is mounted over the driver's compartment which is stowed flat against the roof when not in use. A second drop-down bunk is also installed on the side wall of the driver's side. This bunk is normally stowed flat against the roof when not in use and drops down over the workbench area when needed.

A fully enclosed modular style sanitary facility is installed as indicated in Figure 3-30. The enclosure contains a regular flush type toilet with running water obtained from a 30-gallon supply tank. The toilet empties through a positive shut-off bottom valve into a 26-gallon holding tank. A small corner type wash basin is provided. This installation includes gauges for indicating both the holding tank level and the water supply tank level.

A forced air LP gas fueled furnace is installed for interior heating. The system has a capacity of 30,000 BTU/hour and is controlled by a thermostat for temperature regulation. For self-contained operation, two 30 lb. LP gas tanks are mounted in a compartment accessible from the outside only. A pressure sensitive automatic change-over valve regulates the gas flow to the furnace with provision for connection to an external LP gas source.

In the area immediately adjacent to the sanitary facility and extending rearward to the wheelwell on the driver's side, a countertop and cabinetry are installed to serve as a workbench. In the area immediately adjacent to the generator compartment on the co-driver's side and extending rearward, a countertop and cabinetry are installed to serve as a desk. The system contains ample storage cabinets, drawers, etc., as required for storage of equipment and tools.

The system has two prime electrical circuits, referred to as "Bus A" and "Bus B". Each bus is normally connected to one of the two generators. Bus A is the electrical circuit usually installed within the van from which the environmental systems and standard accessories of the van are powered. This circuit includes both

air-conditioners, circulating fans or blower of the furnace, converter for the 12 volt DC equipment of the van such as the interior lighting fixtures, and 110 volt AC receptacles installed along the side walls of the van. A second prime electrical circuit, known as Bus B, is the electrical circuit from which the project scientific equipment is powered.

Control and distribution of the electric power in the van is from a common panel mounted in a cabinet type enclosure located on the co-driver's side wall between the rear entry door and rear bulkhead as shown in Figure 3-20. Contained on this control panel are facilities for starting and stopping both generators, meters for recording the accumulative running time of both generators, meters to indicate the output voltage and current of both generators, transfer switches to connect the load from Bus A and Bus B to either generator, and provision for transferring the entire load of the van to external public utility AC power. Also contained on the panel are circuit breakers for protecting the various sub-circuits of the AC equipment.

SECTION 4

BIBLIOGRAPHY

1) Brown, R. T., Backscatter Signature Studies for Horizontal and Slant Range Visibility, Final Report No. FAA-RD-67-24, available from DDC: AD-659-469 (1967).

2) Viezee, W., J. Oblanas and R. T. H. Collis, Slant Range Visibility Measurement for Aircraft Landing Operations. Final Report AFCRL No. 72-0154 (1972).

3) Brown, R. T., "A New Lidar for Meteorological Application", J. Appl. Meteor. 12, 698 (1973).

4) Knestrick, G. L. and Curcio, J. A., Measurements of Spectral Radiance of the Horizon Sky, Applied Optics, Vol. 6, No. 12, December 1967.